Physics – Uspekhi **41** (1) 25 – 48 (1998)

REVIEWS OF TOPICAL PROBLEMS PACS numbers: 61.66.Fn, **61.90.+d, 77.22.–d**

Dielectric spectroscopy of hydrogen-bonded crystals, and proton relaxation

M P Tonkonogov

Contents

Abstract. Dielectric spectroscopy of polarization phenomena and electromigration kinetics is fraught with discrepancies. The removal of these discrepancies and the generalization of the available data using the theoretical models introduced here allow the basic features of proton relaxation to be revealed. The features of proton relaxation and conduction are established for ice and then extended to more complex structures such as crystalline hydrates and micas. A theory is advanced which allows proton relaxation in hydrogen-bonded crystals to be explained. Relaxation and electromigration mechanisms as well as the types and parameters of relaxators are established and the electretic properties of micas analyzed.

1. Introduction

Dielectric spectroscopy of crystals implies the experimental determination of the spectra of thermally stimulated depolarization and polarization currents (TSDC and TSPC, respectively) and complex permittivity spectra (ε, $\tan\delta$) as well as theoretical analysis of them using kinetic equations and computational methods of mathematics [1 – 5]. Dielectric spectroscopy has been successfully applied to the investigation of real crystal structures like alkali – halide crystals. However, studies of hydrogen-bonded crystals are hampered by the difficulties encountered in the construction of polarization and carrier transport theory. N Bjerrum suggested the concept of ice structural defects and thus made the first step towards examining hydrogen-bonded crystals. H Gränicher used Bjerrum's ideas to explain electrical conduction and polarization in ice. C Jaccard and M Hubmann proposed a phenomenological theory of ice electric properties.

Thousands of papers on the electrophysics of ice have been published during the last half-century. The present review summarizes the most interesting and important ones. Our purpose was to exclude from consideration any doubtful facts when discussing a large number of conflicting experimental findings, select the most valuable data, provide an adequate theoretical interpretation, and elucidate mechanisms of polarization and carrier transport.

Materials containing hydrogen bonds are considered to be of special value for technical needs largely by virtue of their excellent insulating properties (micas, talc, kaolin). They can be used to ensure insulation under extreme conditions (strong fields, high frequencies and temperatures, and ultrasonic effects). This brings up the necessity of in-depth studies of the mechanisms underlying dielectric relaxation in crystals with proton conduction. The ideal material for this purpose is single-crystalline ice wherein the proton relaxation along hydrogen bonds manifests itself as the migration of ionization (H_3O^+, OH^-) and orientation (L, D) structural defects (Bjerrum defects).

The physical aspects of the theory of thermally stimulated currents (TSC) in ice developed in the present review pertain to the comparison of experimental and computed spectra and are intended to facilitate an understanding of the mechanism responsible for TSC origin as a result of the breakdown of hetero- and homocharges.

M.P. Tonkonogov Department of Physics
E A Buketov Karaganda State University
Universitetskaya ul. 28, 470074 Karaganda, Republic of Kazakhstan
Tel. (3212) 58-14 54

Received 5 November 1996
Uspekhi Fizicheskikh Nauk **168** (1) 29 – 54 (1998)
Translated by Yu V Morozov; edited by A Radzig

The present review discusses evidence of the doping effect on TSC in crystalline ice. The ice was doped with HCl which is known to generate L-defects, and NH_4OH giving rise to D-defects. L-defects are actually broken hydrogen bonds devoid of a proton. D-defects are characterized by the presence of two protons on one hydrogen bond. Ice is peculiar in that the configuration vector influences the dynamics of the orientation (L and D) and ionization (H_3O^+, OH^-) structural defects. Research into formation of negative TSDCs helps to understand the electretic properties of ice.

General laws of proton conduction and relaxation established using model ice crystals may be extrapolated to more complicated dielectrics with hydrogen bonds. The majority of current studies on such crystals as micas, talc, kaolin, and gypsum consider polarization and carrier transport regardless of hydrogen bond defects even though proton migration along hydrogen bonds in these crystals constitutes the main relaxation mechanism. Measurements of TSDC and $\tan\delta$ in mica, gypsum, and talc revealed their identity. As ice, these materials show TSDC and $\tan\delta$ maxima caused by relaxation of H_3O^+, OH^-, L- and D-defects and complexes of them and by relaxation of dipoles of adsorbed and structurally bound water.

Of special interest is phlogopite in which negative TSDCs are generated, as in ice, giving rise to the electretic state. Electretic properties of phlogopite may be of great value in industry (memory cells, membranes).

This paper considers dipole relaxation described by a system of differential equations for a crystal model in the form of a set of m potential wells, which permits an analytic solution. The theory explains polarization kinetics and describes the thermal depolarization mechanism.

Proton dielectrics and semiconductors (micas, ice) may prove to possess promising properties at low temperatures when quantum effects become essential (for example, in space).

2. Ice as a proton semiconductor

2.1 Defects of ice crystal structure

In the ice crystal lattice, oxygen atoms form the ordered substructure corresponding to either wurtzite (hexagonal ice) or sphalerite (cubic ice) [6–9]. The electrical properties of ice are characterized by high dielectric constant due to dipole polarization [10–19] and a rather small volume electric conductivity [20–27].

Bernal and Fowler [28] demonstrated that hydrogen atoms in ice are arranged along lines connecting oxygen atoms. This results in:

— one hydrogen atom per hydrogen bond;

— the hydrogen atom being closer to one of the two oxygen atoms;

— there being two hydrogen atoms near each oxygen atom.

Therefore, it is possible to construct $(3/2)^N$ configurations for N molecules [8, 29–31]. Hence, the entropy at zero temperature is $S = k\ln(3/2)^N = 0.8$ cal kmol^{-1}. Measurements [32] around 0 K yield 0.82 ± 0.05 J K^{-1} [33]. The transition from one configuration to another with increasing temperature is infeasible if the Bernal–Fowler rules are fulfilled.

Bjerrum [34] was the first to explain the violation of these rules by the presence of structural defects (Fig. 1). The energy of formation of an orientation defect pair is characterized by the equation

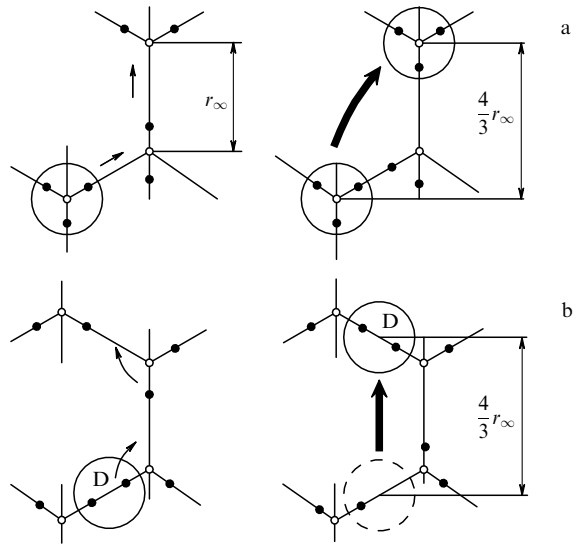

Figure 1. Schematic representation of ion defect (a) and D-defect (b) transitions in hexagonal ice.

$$2\mathrm{H} \rightleftarrows \mathrm{D} + \mathrm{L} + U_0 \,. \tag{2.1}$$

Ionization defects arise from a shift of an H^+ along a hydrogen bond from one oxygen ion to another according to

$$2\mathrm{H_2O} \rightleftarrows \mathrm{OH^-} + \mathrm{H_3O^+} + U_1 \,. \tag{2.2}$$

The activation energy of ion defects is low because of proton tunnelling [21, 35]. Ice crystals contain interstitial H_2O molecules and their vacancies, due to low-density and loose structure [36, 37]. The H_2O stacking factor is 0.34 [38].

Gränicher [38, 39] explained the electrical properties of ice by the migration of structural defects. Fundamental studies by Jaccard [25, 40] on the dynamics of H_3O^+, OH^-, D-, and L-defects allowed him to develop a phenomenological conduction theory for both classical and quantum-mechanical proton transfers. The frequency-dependent permittivity of ice [25, 40] is defined by an analog of the Debye formula

$$\varepsilon' - \mathrm{i}\varepsilon'' = \frac{\varepsilon_S}{1 + \mathrm{i}\omega\tau} \,, \tag{2.3}$$

while the relaxation time τ in (2.3) is determined from a rather complicated equation

$$\frac{1}{\tau} = \left[(\sigma^+ + \sigma^-)\right] \frac{32}{3\sqrt{3}} \left(\frac{er}{pa}\right)^2 + (\sigma^{\mathrm{L}} + \sigma^{\mathrm{D}}) \frac{3\sqrt{3}}{4} \left(\frac{er}{4}\right)^2 \Bigg] \frac{rkT}{e^2} \,. \tag{2.4}$$

The high-frequency volume electric conductivity

$$\sigma_\infty = \sigma^+ + \sigma^- + \sigma^{\mathrm{L}} + \sigma^{\mathrm{D}} \tag{2.5}$$

is due to majority defects responsible for a rather high partial conduction [25]. In (2.3) and (2.4), the following notation was used:

$$\varepsilon_S = \frac{e^2}{\varepsilon_0 rkT} \Gamma \,, \tag{2.6}$$

$$\Gamma = \left\{ \left[\Sigma_{\rm i} \frac{er}{pa} - \Sigma_{\rm o} \frac{er}{2qb} \right] \Sigma_{\rm i} \frac{32}{3\sqrt{3}} \frac{er}{pa} - \Sigma_{\rm o} \frac{3\sqrt{3}}{2} \frac{er}{qb} \right\} \times \left\{ \left[\Sigma_{\rm i} \frac{32}{3\sqrt{3}} \left(\frac{er}{pa} \right)^2 + \Sigma_{\rm o} \frac{3\sqrt{3}}{4} \left(\frac{er}{4} \right) \left(\frac{er}{qb} \right)^2 \right]^2 \right\}^{-1}, \tag{2.7}$$

where $\Sigma_{\rm i} = \sigma^+ + \sigma^-$, and $\Sigma_{\rm o} = \sigma^{\rm L} + \sigma^{\rm D}$.

The conduction in a static electric field (low-frequency conduction) is defined by a minority charge carriers [25]:

$$\frac{1}{\sigma_{\rm o}} = \frac{1}{\Sigma_{\rm i}} \left(\frac{pa}{er} \right)^2 \left(1 + \frac{10}{27} \frac{qb}{er} \right)^{-1} + \frac{1}{\Sigma_{\rm o}} \frac{128}{27} \left(\frac{qb}{er} \right)^2 \times \left(1 + \frac{10}{27} \frac{qb}{er} \right)^{-1}. \tag{2.8}$$

Here, σ^i is the partial volume electric conductivity of defects ($i = H_3O^+$, OH^-, D, L); p and q are the effective charges of ion and orientation defects (it should be borne in mind that $p \neq q$); b is the distance between oxygen ion and the nearest proton; $r = a + 2b$; e is the proton charge, and a is the distance between protons on the same hydrogen bond.

Neither the conductivity nor dielectric constant shows a frequency dependence if the low- and high-frequency electric conductivities are equal in the narrow region of the so-called 'cross-over' [41, 42] (Fig. 2). In that event $\sigma_0 = \sigma_\infty$. The existence of 'cross-over' explains results of a large body of research [9, 24, 43–47]. It follows from the Jaccard theory [25] that the principal mechanism of charge transfer in pure ice crystals is associated with orientation defects. Theoretical estimates of the mobility of ion and orientation defects are in good agreement with experimental findings [48]. Jaccard was the first to introduce the configuration vector $\mathbf{\Omega}$ [40] which allowed for a specific direction in space of hydrogen bonds to be taken into consideration:

$$\mathbf{\Omega} = \int_0^T (\mathbf{j}_1 - \mathbf{j}_2 - \mathbf{j}_3 + \mathbf{j}_4)\, {\rm d}t = \int_0^T \sum_{k=1}^{4} \eta_k \mathbf{j}_k \, {\rm d}t\,. \tag{2.9}$$

Here, $\mathbf{\Omega}$ characterizes the flow of defects; $\eta_k = +1, -1, +1, -1$ for H_3O^+, OH^-, D, and L, respectively, and $\mathbf{j}_k = \mathbf{v}_k n_k$ are their partial fluxes.

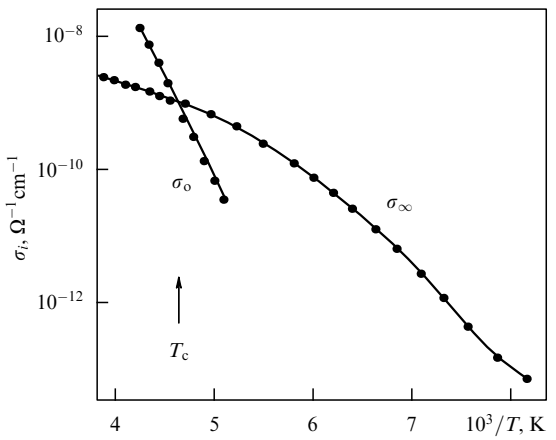

Figure 2. Temperature dependences of low-frequency (σ_o) and high-frequency (σ_∞) conductivities intercepting at the 'cross-over' temperature T_c [18].

A proton shift along or between hydrogen bonds means a jump of the defect by Δl. The modulus of the configuration vector is equivalent to the product of Δl and the quantity v which is actually the difference in the number of protons displaced along the electric field and in the opposite direction [40]:

$$|\mathbf{\Omega}| = v\Delta l\,,$$

where

$$\Delta l = \frac{4r_\infty}{3}\,, \qquad r_\infty = 2.65 \times 10^{-10}\ {\rm m}.$$

The Jaccard theory was further developed in a work by Hubmann [71], who examined a broad spectrum of defects including (H_3O^+, L) and (OH^-, D) complexes.

Kryachko [72] denied the existence of Bjerrum defects and suggested a king-soliton model of orientation defects in the hydrogen-bond network of ice crystals. A king-soliton is a stable transient state between the H_2O subsystem, where all OH^--dipoles are at a minimum position with the angle $\Theta = -\Theta_e$, and the H_2O subsystem in which all dipoles occupy the equivalent positions with $\Theta = \Theta_e$. However, the cooperative mechanism suggested by Kryachko does not explain the results of measuring a complex permittivity, thermally stimulated currents, and electric conduction. The existence of a king-soliton in ice was not confirmed by experiment.

2.2 Complex permittivity and volume electric conductivity of ice

Many authors offer similar interpretations of complex permittivity spectra in ice (Fig. 3) [11, 49–53, 45, 42, 24, 14, 15, 17]. The temperature dependence of the dielectric relaxation time is shown in Fig. 4 [53]. The experimentally found activation energy above 223 K is 0.575 eV, in agreement with [11]. However, Ref. [15] reports a different activation energy of 0.23 eV at around 223 K [54]. This latter energy used to be related to the diffusion of L-defects; its value is consistent with Jaccard's calculations [40]. The activation energy measured above 223 K may be compared with the activation energies obtained from measurements of ice internal friction (0.58 ± 0.02 eV) [55], proton spin-lattice relaxation (0.611 ± 0.004 eV, 0.58 eV) [56, 57], and the diffusion of hydrogen and oxygen atoms (0.63 ± 0.04 eV, and 0.67 ± 0.08 eV) [36].

Measurements of ice's heat capacity [29, 58] and residual entropy [29, 31] at a low temperature suggest that H_2O molecules are orientationally disordered in ordinary hexagonal ice. This inference is confirmed by neutron diffraction and IR ice spectra [8, 59]. Also, the ferroelectric phase transition in low-temperature ice was assumed to occur on fulfilling the Curie–Weiss law [14, 15, 46, 53, 54, 60–64]:

$$\varepsilon_{\rm o} - \varepsilon_\infty = \frac{A}{T - T_{\rm C}}\,, \tag{2.10}$$

where $T_{\rm C}$ is the Curie temperature. Such a transition at $T < 100$ K must have resulted in a jump of heat capacity [66] and a fall in entropy to below 0.1 J kmol^{-1} [65–70], which were never confirmed.

Ref. [14] describes the distribution of relaxation times in the temperature range from 165 to 250 K, whereas only one relaxation time was recorded at $T > 250$ K [62]. According to Ref. [54], the smearing of the relaxation time spectrum is due

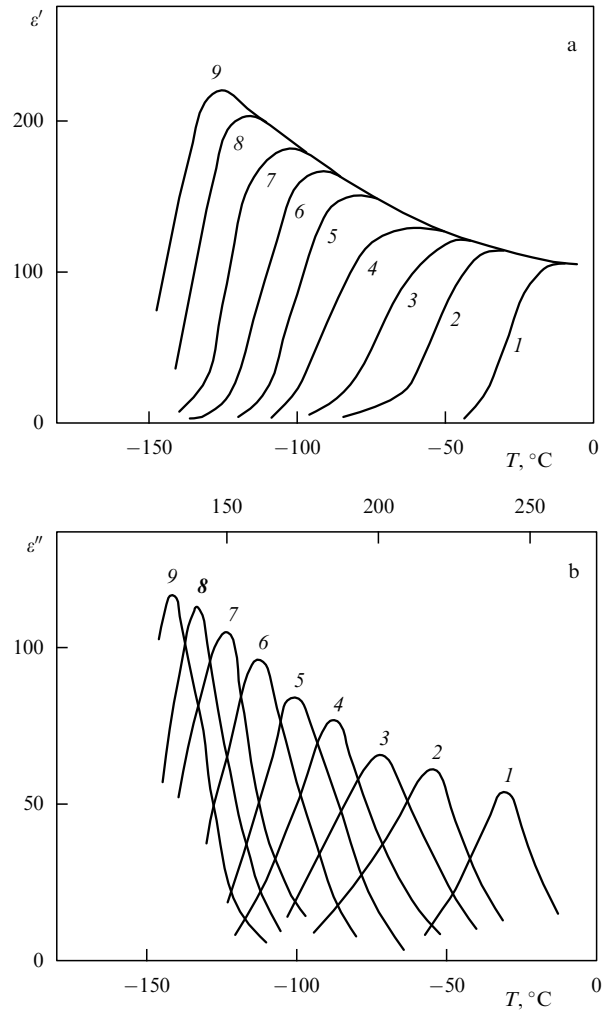

Figure 3. Temperature-frequency spectra of real (a) and complex (b) parts of the permittivity of pure single-crystalline ice (||C): *1* — 0.3 kHz; *2* — 100 Hz; *3* — 30 Hz; *4* — 10 Hz; *5* — 3 Hz; *6* — 1 Hz; *7* — 0.3 Hz; *8* — 0.1 Hz; *9* — 0.03 Hz [15].

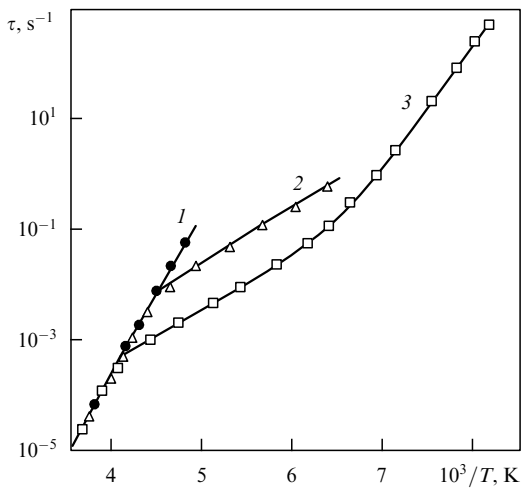

Figure 4. Temperature dependence of relaxation time in pure ice: *1* — single-crystalline ice [11]; *2* — single-crystalline ice [15]; *3* — polycrystalline ice [14].

to the presence of chemical impurities and structural inclusions in the crystal.

Certain authors have tried to derive the constant in the Curie – Weiss law from permittivity spectra [15, 60, 61, 64]. The anisotropy in the directions parallel and perpendicular to the axis C was found to be around 13% and 21%, respectively, near the melting point. At 123 K, it was 41% for H_2O and 48% for D_2O [15 – 63]. The anisotropy of the permittivity found in [53] near the melting point did not exceed 10%, whereas it was only 1% in the temperature range of 200 – 273 K [62]. According to [15, 16, 63], the Curie – Weiss temperature for H_2O and D_2O came out to 0 K when the electric field vector was normal to the axis C, and 46 and 55 K when it was parallel to the same axis. This obvious discrepancy questions the existence of the ferroelectric transition.

Theoretical studies of ice's dielectric properties at the atomic level have actually been of a semiphenomenological nature [6, 25, 40, 41, 71, 73 – 76]. They demonstrated that hydrostatic pressure affects ε [47]. Also, they provided evidence of dipole polarization changes by the action of mechanical tension and the documented effect of ice crystal ageing on dielectric properties [77]. This effect was examined by measuring ice density [78], coefficient of elasticity [79], and proton spin-lattice relaxation [80]. The effect of crystal ageing on ice dielectric properties was investigated in Refs [49, 77, 81 – 86]. These studies revealed the time dependence of low-frequency dispersion. Progressive separation of the Debye and low-frequency dispersions with time was related to the thinning down of the quasi-liquid layer covering the ice surface [21, 49, 87 – 89], which is believed to occupy the intercrystallite space [49, 86, 90 – 92]. The high probability of this was postulated in Refs [86, 31 – 96].

If U_1 is the activation energy related to the formation of a pair of orientation (D, L) defects and U_2 is the activation energy of reorientation of H_2O molecules due to migration of L-defects, then the activation energy of the relaxation process takes the form

$$U = U_2 + \frac{U_1}{2} \,. \tag{2.11}$$

Some authors have reported $U_1 = 0.685$ and $U_2 = 0.238$ eV [23, 25]. In highly purified crystals at temperatures below 210 K, the activation energy falls down to 0.26 eV [14 – 16, 18, 53, 54, 61]. It has been suggested that equilibrium Bjerrum defects make the greatest contribution to dielectric relaxation at high temperatures, whereas defects related to impurities and structural inclusions play a major role at low temperatures [47]. Refs [41, 44] attribute the variation of activation energy to the transfer from the motion of orientation defects prevailing at high temperatures to that of ionization defects at low temperatures, in compliance with what was shown in Ref. [21]. The activation energy of 0.256 eV [14] corresponding to an L-defect agrees satisfactorily with the activation energies of 0.238 and 0.29 eV obtained in Refs [23, 25]. Decreasing the temperature to around 150 K once again changes the slope of the temperature dependence of relaxation time. According to [61], the mechanism of H_2O molecule reorientation in this temperature region varies, being shifted from reorientation of individual molecules at high temperatures to collective reorientation at low temperatures. The Debye dispersion region was scrutinized in Refs [14, 16, 43, 54, 97 – 99]. The effects of volume charge in pure and doped ice were discussed in works [17, 24, 46, 53, 95, 100, 101].

It is of certain interest to consider the temperature dependences of low- and high-frequency volume electric conductivities in pure and doped ice [23, 71, 44]:

$$\sigma_\infty = \sigma_\pm \pm \sigma_{\mathrm{DL}}\,, \tag{2.12}$$

$$\frac{(e_\pm + e_{\mathrm{DL}})^2}{\sigma_{\mathrm{o}}} = \frac{e_{\mathrm{DL}}^2}{\sigma_{\mathrm{DL}}} + \frac{e_\pm^2}{\sigma_\pm}\,. \tag{2.13}$$

Complexes involving one positive ion defect and one negative orientation defect (H_3O^+, L) were discussed in Ref. [64], where their strong fixation in the crystal lattice was disclaimed while the diffusion of H_3O^+ and L defects is supposed to make a major contribution to the dielectric polarization and conduction in ice. This view is shared by the authors of Refs [23, 41] who believe that such complexes must show properties of ionization defects and, under certain conditions, play the definitive role in dielectric relaxation notwithstanding the involvement of L-defects in their motion. The same authors proposed models to calculate the temperature spectra of volume electric conductivities σ_{o}, σ_∞; the data obtained proved to be consistent with experimental findings. They also considered the generation of a free L-defect and ion defects by each HF molecule at concentrations satisfying (in accordance with the law of mass action) the relation

$$\frac{(n_{\mathrm{H_3O^+}})^2}{n_{\mathrm{F}}} - n_{\mathrm{H_3O^+}} = K\,, \tag{2.14}$$

where n_{F} is the concentration of F, and $K = \mathrm{const}$. At relatively high concentrations one obtains

$$n_{\mathrm{H_3O^+}} \propto \sqrt{n_{\mathrm{F}}}\,. \tag{2.15}$$

A similar defect diffusion mechanism has been considered in alkali – halide crystals [102, 103].

The fulfillment of relation (2.4) was confirmed by the dependence

$$\sigma_{\mathrm{o}} \propto \sqrt{n_{\mathrm{F}}} \tag{2.16}$$

experimentally established at relatively high HF concentrations; at low n_{F} concentrations, σ_{o} and n_{F} values turned out yet to be proportional [25, 104, 105]. In addition to the role of (H_3O^+, L) complexes in dielectric relaxation, the authors of Ref. [41] noticed a change in the mechanism of motion for the majority and minority charge carriers at the 'cross-over' temperature [9, 18, 77, 106 – 109]. The 'cross-over' condition is illustrated by Fig. 2. Since the activation energy of low-frequency conductivity exceeds that of high-frequency conductivity, the 'cross-over' may be absent in pure ice crystals. At T_{c}, when the mechanism of motion of majority and minority defects undergoes alteration, partial fluxes of ion and orientation defects become identical (see Fig. 2):

$$\frac{\sigma_{\mathrm{i}}}{p} = \frac{\sigma_{\mathrm{B}}}{q}\,. \tag{2.17}$$

According to [110] we have

$$\varepsilon - \varepsilon_\infty = \frac{\varepsilon_S - \varepsilon_\infty}{1 + \mathrm{i}\omega\tau}\,, \tag{2.18}$$

and it is possible to write down

$$(\sigma_\infty - \sigma_{\mathrm{o}})\tau = \varepsilon_{\mathrm{o}}(\varepsilon_S - \varepsilon_\infty) = \varepsilon_{\mathrm{o}}\Delta\varepsilon \tag{2.19}$$

for the volume electric conductivity. In the case of the 'cross-over'

$$\sigma_{\mathrm{o}} = \sigma_{\mathrm{B}} + \sigma_{\mathrm{i}}\,. \tag{2.20}$$

The analysis in Ref. [41] demonstrated that the 'cross-over' appears at equal concentrations of an impurity and the Bjerrum defects it generates. Two 'cross-overs' are likely to arise when the HF impurity undergoes not total dissociation [41].

The dielectric characteristics of ice containing HF impurity have been investigated over broad temperature and frequency ranges [23, 24, 43, 111], whereas the properties of HCl-doped ice are poorly known.

The complex permittivity spectra of ice have been examined at 20 Hz – 20 kHz frequencies over a relatively narrow concentration range of $2 \times 10^{-6} - 2 \times 10^{-4}$ M HCl [95]. The results obtained at high temperatures proved to be in line with those reported in Refs [11, 12, 112] and were later confirmed at a sufficiently high level of HCl impurity [113]. The similarity of complex ε spectra in HCl- and HF-doped ice was demonstrated in [25, 42, 65, 113, 114]. The concentration dependence of the volume electric conductivity at low impurity levels ($< 10^{-4}$ M) observed at low frequencies turned out to be at variance with that obtained in [115], where the minimum in volume electric conductivity was found. Ref. [100] concerned the temperature dependences of low (σ_{o})- and high (σ_∞)-frequency volume electric conductivities, Debye and migration relaxation time spectra, and the temperature region adjacent to the 'cross-over' T_{c} in HCl-doped ice single crystals in a narrow concentration range of $10^{-5} - 10^{-4}$ M. In this case, σ_{o} was proportional to the HCl concentrations and showed no temperature dependence at $T > T_{\mathrm{c}}$ due to total dissociation of the molecular admixture (HCl), which generated ion defects (H_3O^+) in the crystal lattice. At $T < T_{\mathrm{c}}$, the dependences had the form

$$\sigma_\infty\,, \quad \sigma_{\mathrm{o}} \propto \sqrt{n_{\mathrm{HCl}}}\,.$$

Such behaviour of the temperature and concentration dependences of σ_{o} was in conformity with previous observations [24, 43], although the characteristics of the σ_∞ spectra were at variance with those found in an early study [116]. Also, the temperature dependence of the conduction activation energy was shown to have anomalous patterns. The value of U_σ turned out to be 0.3 eV [25, 42, 104] regardless of the impurity level in the range from 10^{-5} to 10^{-2} M HF. According to [117], a similar behaviour for U_σ was observed in HCl-doped ice. On the other hand, one more study [95] revealed a concentration dependence of U_σ. And similar results were obtained for HF-doped ice [115]. In the latter case, the minimum of U_σ occurred at an impurity level of $\sim 1 \times 10^{-4}$ M. Such a discrepancy between the measurements of complex σ and ε was characteristic of both pure and doped ice [12, 20, 22, 25, 26, 118 – 121]. The experimentally found dielectric properties of pure and doped ice in an alternating current, the existence of the 'cross-over', and the presence of low-frequency Maxwellian relaxation were readily described by phenomenological computation [23, 25, 40, 71, 122] based on the Jaccard theory. The reasons for significant discrepancy between measured results have to do with the following:

— the dielectric properties of ice are affected by crystal growth and specimen annealing conditions [77, 123], and

— it is difficult to obtain nonblocking contacts for ice [124].

In [20], platinum electrodes were used, overlaid with a hydrogen-saturated palladium film. The use of hydrogen-saturated palladium was also recommended in Ref. [125]. Jaccard [25] obtained electrodes by evaporating gold in a high

vacuum, while the authors of Ref. [42] used the so-called 'sandwich' electrodes of HF-doped ice in which the impurity level was almost 10 times that in the sample. Proton electrodes were proposed in [126], however their quality was questioned [127, 128].

The use of blocking electrodes to measure the complex permittivity of ice resulted in a volume charge around them which accounted for the overestimation of the real part of the dielectric constant at superlow frequencies. According to [95, 129], a volume charge can influence dielectric properties of ice through the presence of dissolved air bubbles. The volume charge impact on the permittivity spectrum was documented in Refs [23, 42, 100, 130, 131].

A rise in temperature ($T > 240$ K) enhances the role of surface electrical conduction which dims the measurements of dielectric parameters [18, 96, 108, 132, 133]. It has been demonstrated both in theory and experiment [96, 132] that in this case the ice surface is a quasi-liquid layer. Ref. [44] recommends measuring the ice dielectric characteristics in an inert gas. Measurements in a vacuum are attended by the continuous sublimation of H_2O molecules and the inflow of the defects to the surface of the crystal which impairs reproducibility. The choice and preparation of electrodes are crucial for measuring the dielectric parameters of ice.

Analysis of the experimental dielectric characteristics of ice has shown that both current measuring techniques and the theoretical interpretation of the results are imperfect. Special attention should be given to near-electrode polarization and surface conduction which are apt to mask the real values of the volume electric conductivity and the complex permittivity. These requirements were met in Ref. [134]. Temperature vs. frequency curves of $\tan\delta$ are available for ice polycrystals (Fig. 5). The $\ln\tau$ dependence on $10^3/T$ (see Fig. 6) has two slopes (curve *1*) corresponding to activation energies of $U_1 = 0.63 \pm 0.08$ eV and $U_2 = 0.25 \pm 0.05$ eV. Spectra *2–5* appear to occur in a higher-frequency region than spectrum *1*, probably due to effect of the volume charge field on the relaxation time spectrum. The existence of a set of relaxation times at lower temperatures is confirmed by the Cole and Cole plots (Fig. 7) at 262, 253, and 247 K (curves *1*, *2*, and *3*, respectively), which are impossible to separate based on dielectric losses. The Cole and Cole plots imply at least three sets of relaxators.

To summarize, $\tan\delta$ and ε spectra bear incomplete information about the types and parameters of relaxators in ice.

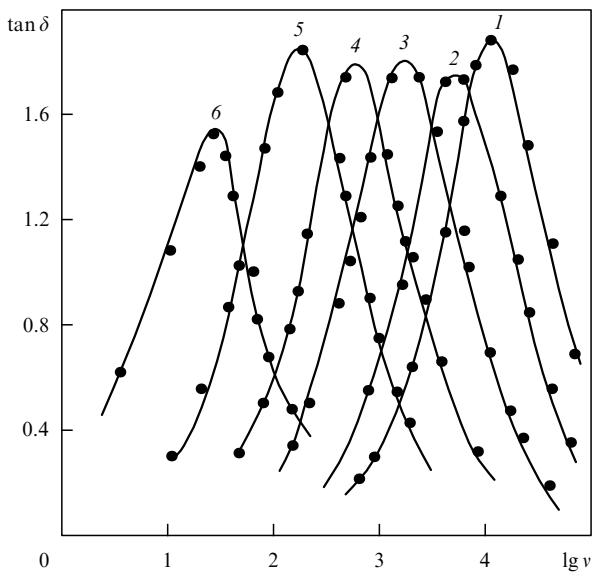

Figure 5. Frequency dependences of $\tan\delta$ in pure polycrystalline ice at different temperatures: *1* — $T = 263$ K; *2* — $T = 256$ K; *3* — $T = 247$ K; *4* — $T = 240$ K; *5* — $T = 230$ K; *6* — $T = 200$ K [134].

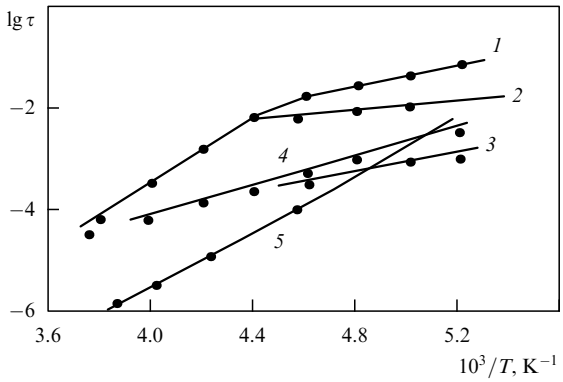

Figure 6. Relaxation time spectra obtained by $\tan\delta$ (curve *1*) and TSC (curves *2–5*) measurements: *2* — $U_1 = 0.1$ eV, $\tau_{01} = 3 \times 10^{-5}$ s; *3* — $U_2 = 0.23$ eV, $\tau_{02} = 1.73 \times 10^{-9}$ s; *4* — $U_3 = 0.28$ eV, $\tau_{03} = 1.8 \times 10^{-10}$ s; *5* — $U_4 = 0.5$ eV, $\tau_{04} = 2.5 \times 10^{-16}$ s [134].

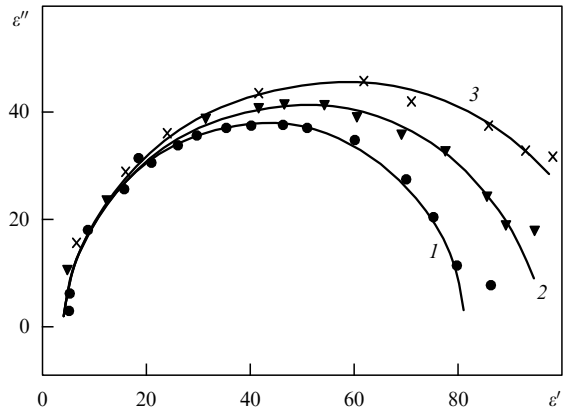

Figure 7. Cole and Cole plots for ice [134].

2.3 Thermally stimulated currents (TSC) in ice

The depolarization TSC technique is based on the polarization of a dielectric specimen in an electric field at a sufficiently high temperature during a period longer than the relaxation time, followed by rapid cooling, removal of the polarizing field, closing the dielectric/electrometer circuit and, finally, measuring the electric current which passes through the specimen [10]. The temperature dependence of TSC may feature several peaks corresponding to the relaxation of selected groups of defects. To measure TSPC spectra, the dielectric is first cooled in the absence of an electric field, then the field is applied and the current through the sample is measured, whilst being heated. The temperature dependence of polarization TSC also displays several maxima. The resolution of the TSC method allows groups of relaxators to be separated which is not an easy task when dealing with an alternating current. The TSC technique has wider application

for the analysis of relaxation time spectra than $\tan\delta$ and ε measurements, since TSC measuring instruments ensure a 100 times higher accuracy of reading than that achieved by measuring the Q-factor of contours. Moreover, measurement of the TSC, unlike that of $\tan\delta$, does not require tuning to the fundamental polarization harmonic.

The TSDC curve for pure ice normally shows two main current peaks at around 120 and 220 K [10, 60, 97, 135–141]. In an early work by Dengel et al. [142], the low-temperature (LT) current maximum was apparent at 110 K. Then a change in the current direction was observed and a minimum at 125 K manifested itself, which the authors tried to relate to the ferroelectric transition near 100 K. In the neighbourhood of this temperature, there occurred jumplike changes of heat capacity [68, 143], Young's modulus [144], and polarization [13, 145–148] in both pure and HF-doped ice. In [149], the nature of the LT maximum of TSDC was accounted for by trapping Bjerrum defects in the lattice and their subsequent thermally induced release upon heating of the specimen.

The TSPC spectra in HF-doped ice showed maxima at around 100 and 125 K [150]. The LT peak shifted to a lower temperature region with growing HF levels. The LT peak of TSPC was attributed to the relaxation of H_2O dipoles due to the migration of L-defects [150]. According to [25, 40], the relaxation time depends on the concentration of L-defects, i.e. on HF levels:

$$\frac{1}{\tau} \propto n_{\mathrm{L}} \,. \tag{2.21}$$

It follows from (2.21) that the TSC peak shifts to a lower temperature region with growing HF levels. In [150], the TSDC spectrum in HF-doped ice ($n_{\mathrm{HF}} = 9 \times 10^{22}$ m^{-3}) showed peaks at the same temperatures. However, the second TSC peak was followed by a negative current minimum at around 138 K. The general shape of the TSC spectrum in Ref. [150], for instance, the presence of the current maximum and minimum, and their temperature-dependent positions were consistent with the data of [142] and could be accounted for by the ferroelectric transition. However, the authors of [142] explained the TSC minima by the processes in ice near the electrodes. The possibility of transition of the ice's crystal structure to the ferroelectric phase was assessed by the TSC method in Refs [13, 145, 151, 152].

The relaxation of H_2O dipoles caused by the migration of L-defects and responsible for the LT maximum of TSC was considered in [97, 114, 135–141, 153]. At the same time, the authors of Ref. [151] attributed the thermally stimulated depolarization currents at 125 K to volume-charge phenomena at the blocking electrodes. On the other hand, an LT maximum of TSDC occurred when both blocking and gold-sputtered electrodes were used [135].

The results of TSC measurements in pure and doped ice used to be interpreted solely by applying the Bucci and Fieschi formula [154] and the Curie–Weiss law [60]. It should be emphasized that the configuration vector would be equally helpful in the interpretation of experiments with ice as a proton semiconductor.

Ref. [151] considers the parameters of two additional relaxation processes in ice presenting with TSDC maxima around 150 and 160 K, with activation energies of 0.28 and 0.6 eV and frequency factors 1.2×10^{-8} and 5×10^{-17} s^{-1}, respectively. The shape of the experimental LT peak was fairly well described by the Bucci and Fieschi formula [154]. At the same time, the authors of Ref. [60] identified two or even three relaxation processes giving rise to the LT maximum of TSDC. According to [137], the parameters of this maximum were unaffected by the water purity, whereas the authors of Ref. [150] maintained that they depend on HF doping. Furthermore, the LT maximum was shown to be proportional to the strength E_{p} of the polarizing electric field, whereas the position of the LT peak T_{m} turned out to be independent of either E_{p} or the polarization temperature T_{p} [137, 138]. The parameters of LT maxima for single- and polycrystalline ice samples were reported to be stable [137]. The concentration of defects in polycrystal samples increased due to the presence of grain boundaries, dislocations, and inclusions. It was inferred in Ref. [137] that LT dielectric relaxation was independent of the external defect concentration. Investigations of the TSC dependence for ice single crystals doped with HF revealed a current peak at 107 K [145]. The authors explained the presence of this peak by ionization H_3O^+ defects generated by the HF impurity.

On the one hand, the TSC maximum near 220 K used to be attributed to volume charge dissipation [152]. On the other hand, this maximum was approximately described by the Bucci and Fieschi formula [154] and defined as a monorelaxation peak [136]. Ref. [142] demonstrated the participation of ion defects in high-temperature relaxation processes, whereas Ref. [148] reported the contribution of the ionization defect relaxation to a TSC peak at 107 K.

To summarize, there are conflicting interpretations of TSC spectra in the scientific literature, and the mechanisms of relaxation processes in ice remain conjectural.

Ref. [134] reports recent TSC measurements in ice.

A typical TSC spectrum for polycrystalline ice is shown in Fig. 8. TSC peaks can be seen at 127, 139, 158, and 230 K under a heating rate of $c = 2.4$ K min^{-1}. The nonlinear dependence of $\ln I$ on $10^3/T$ for the LT peak was established in [155]. Ref. [60] considers the probable contribution of three different relaxation processes to the LT maximum. The authors managed for the first time to explicitly obtain a current maximum in pure ice with $U_1 = 0.1 \pm 0.01$ eV, $\tau_{01} = 3 \times 10^{-5}$ s at 97 K (peak 1) at the leading edge of the LT peak. This maximum failed to be seen by other authors

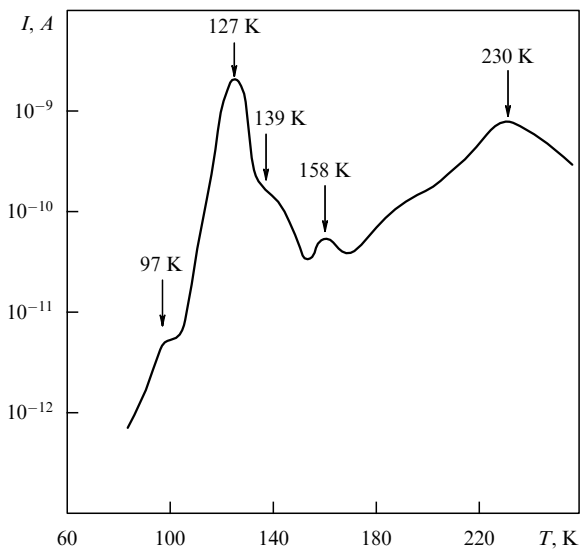

Figure 8. TSC spectrum of polycrystalline ice at a polarizing field strength $E_{\mathrm{p}} = 1.5 \times 10^5$ V m^{-1}, polarization temperature $T_{\mathrm{p}} = 240$ K, polarization time $t_{\mathrm{p}} = 15$ min, and heating rate $c = 4 \times 10^{-2}$ K s^{-1} [134].

Table 1. Parameters of TSDC maxima in ice.

Peak No.	T_m, K	U, eV	$\tau_{0\,\mathrm{expt}}(T_m)$, s	$j(T)_{max}$, A m^{-2}	$P_{0\,\mathrm{calc}}$, C m^{-2}	$\tau_{0\,\mathrm{calc}}$, (T_m), s
1	97	0.1±0.01	3.0×10^{-5}	1.03×10^{-9}	0.1×10^{-7}	3.0×10^{-5}
2	127	0.23±0.01	1.73×10^{-9}	3.0×10^{-7}	0.2×10^{-5}	1.73×10^{-9}
3	139	0.28±0.06	1.8×10^{-10}	4.8×10^{-8}	0.38×10^{-6}	1.8×10^{-10}
4	158	0.5±0.1	2.5×10^{-16}	6.0×10^{-8}	0.31×10^{-6}	1.6×10^{-16}

because of the superposition of a stronger relaxation process at 127 K (peak 2) with $U_2 = 0.23 \pm 0.01$ eV, $\tau_{02} = 1.73 \times 10^{-9}$ s due to a higher concentration of L-defects influencing the position of the peak [60, 135].

Peak 1 appears to be due to the tunnelling of ion H_3O^+ defects whose mobility is slightly dependent on temperature. No TSC maxima were found in Ref. [156] in the range from helium temperature to 90 K. The authors also assumed that the charge calculated from the maximum parameters is proportional to the square root of the HF concentration. Based on this assumption, they considered the quantum-mechanical character of H_2O-dipole reorientation by ionization H_3O^+ defects. In this experiment, the same maximum also occurred in pure polycrystalline ice.

Parameters of the current maxima at 139 K (peak 3) and 158 K (peak 4) with activation energies $U_3 = 0.28 \pm 0.06$ eV and $U_4 = 0.5 \pm 0.1$ eV, while $\tau_{03} = 1.8 \times 10^{-10}$ s and $\tau_{04} = 2.5 \times 10^{-16}$ s, respectively, were obtained by thermal purification. The change in the peak 3 temperature (T_m) for different samples did not exceed ±3 K, and that for peak 4, at most, ±5 K. The activation energy of peak 2 ($U_2 = 0.23 \pm 0.01$ eV) agreed closely with that ($U = 0.235$ eV) obtained by Jaccard [25] for the diffusion of L-defects.

The measured values proved to be in good agreement with the computed ones. The characteristic parameters of peaks 1–4 are presented in Table 1. The calculations were made using the equation which governs TSDC [10, 154]:

$$j(T) = \frac{P_0}{\tau_0} \exp\left(-\frac{U}{kT}\right) \exp\left[-\frac{1}{c\tau_0}\int_{T_0}^{T} \exp\left(-\frac{U}{kT'}\right) \mathrm{d}T'\right], \tag{2.22}$$

where P_0 is the initial polarization intensity, τ_0 the frequency factor, U the activation energy, and c the heating rate.

The permittivity of ice at $T = 130$ K was calculated from the characteristics of peak 2 using formula

$$\varepsilon_S - \varepsilon_\infty = \frac{Q}{S\varepsilon_0 E_p}\,, \tag{2.23}$$

where S is the sample area, and E_p is the strength of the polarizing field. The total depolarization charge is numerically equivalent to the area enclosed by the peak 2 curve:

$$Q = \int_0^\infty I\,\mathrm{d}t\,. \tag{2.24}$$

The quantity $\varepsilon_S - \varepsilon_\infty$ was 140 ± 10. According to Ref. [46], $\varepsilon_S \approx 130$ in an ice single crystal at $T = 130$ K. Calculations following Jaccard [25] and Hubmann [71] and assuming the orientation polarization of H_2O molecules to be due to the drift of L-defects, gave $\varepsilon_S - \varepsilon_\infty = 162$ as an estimate [135]. In polycrystalline ice, $\varepsilon_S - \varepsilon_\infty \approx 192$ at 135 K [14]. The observed $\varepsilon_S - \varepsilon_\infty$ value is in fairly good agreement with the above theoretical and experimental findings and confirms the orientational nature of peak 2.

The concentration of Bjerrum defects obtained from the relation $N_B = P/(e_B d)$ was $\sim 9.4 \times 10^{17}$ m^{-3}, whereas the number density of oriented H_2O molecules, $n_{H_2O} = P/\mu$, reached 1.6×10^{25} m^{-3} (here P is the polarization intensity of the sample; e_B is the effective charge of Bjerrum defects equal to $0.38e$; d is the crystal thickness, and μ is the dipole moment of an H_2O molecule).

Repeating the TSC measurements on one sample resulted in a shift of T_m for peak 2 to the lower temperature region (down to 116.5 K) due to the increased Bjerrum defect concentration with crystal ageing [150].

It appears safe to argue that the TSC spectra in single- and polycrystalline ice give evidence of four groups of relaxators and provide far more information about proton migration than complex permittivity spectra. The Cole and Cole diagrams also support the existence of relaxator groups. Such relaxators are H_3O^+ (first TSC maximum), L-defects (second TSC maximum), H_2O and OH^- (third and fourth TSC maxima). The D-defects appear to contribute to the third and fourth maxima which are close to each other, the more so that one plot in Fig. 7 may correspond to several sets of relaxators. Peaks 1–4 in TSC spectra are independent of the polarization temperature T_p, whereas peak 5 exhibits a dependence on T_p, which indicates that it is due to the volume charge [10]. This polarization mechanism can be verified by doping ice crystals with impurities capable of altering the concentration of Bjerrum defects. The concentration of L-defects in pure ice is 10^{18} m^{-3} [137, 138] and NH_4OH doping diminishes the L-concentration through the defect annihilation. A similar fall may be expected to occur in the n_{OH^-} level with increasing n_{NH_3}. The possibility of selectively manipulating concentrations of individual structural defects allows the mechanism of their action on TSC spectra to be elucidated. As n_{HCl} increases, peak 2 shifts to the lower temperature region, in conformity with (2.21). The location of peak 1 at low HCl levels ($< 5 \times 10^{-5}$ M) remains unaltered, whereas at a higher concentration ($> 5 \times 10^{-5}$ M) it shifts to the higher temperature region (Fig. 9). Figure 10 shows a series of TSDC

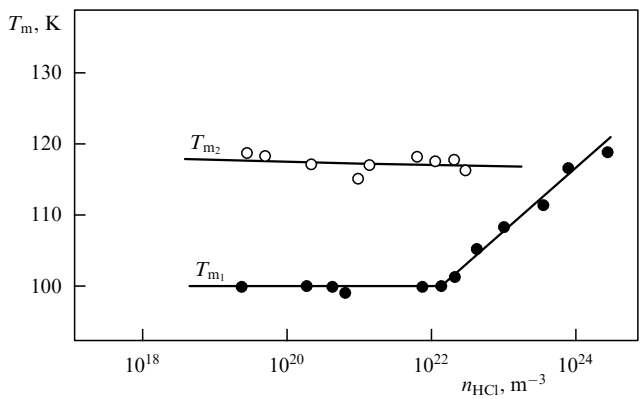

Figure 9. Temperatures of TSDC peaks 1 and 2 as functions of n_{HCl} in pure ice [157].

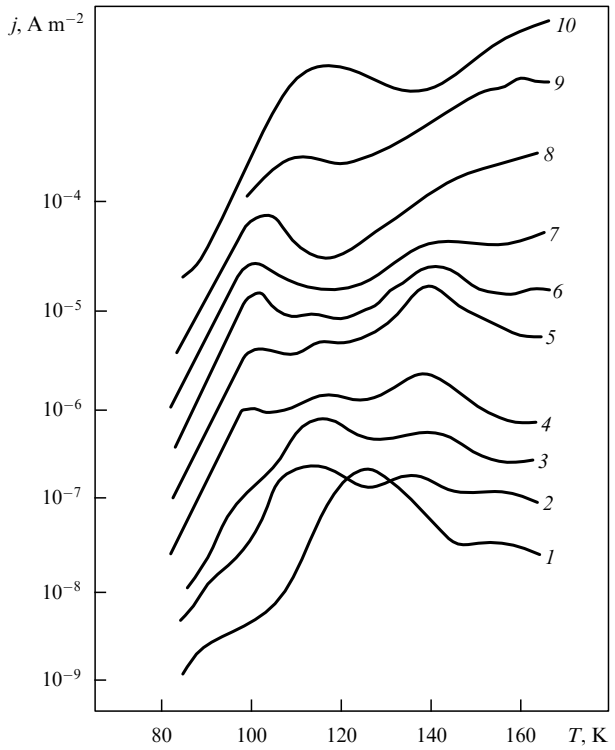

Figure 10. Temperature dependence of TSDC density at different n_{HCl} levels in ice ($E_p = 10^5$ V m^{-1}, $T_p = 240$ K, $t_p = 15$ min, and $c = 4 \times 10^{-2}$ K s^{-1}) [157]: *1* — pure ice; *2* — $n_{HCl} = 4.8 \times 10^{-7}$ M; *3* — $n_{HCl} = 8.48 \times 10^{-7}$ M; *4* — $n_{HCl} = 1.7 \times 10^{-6}$ M; *5* — $n_{HCl} = 5 \times 10^{-6}$ M; *6* — $n_{HCl} = 1 \times 10^{-5}$ M; *7* — $n_{HCl} = 2.5 \times 10^{-5}$ M; *8* — $n_{HCl} = 4.88 \times 10^{-5}$ M; *9* — $n_{HCl} = 9.3 \times 10^{-5}$ M, and *10* — $n_{HCl} = 1.2 \times 10^{-3}$ M.

vs. n_{HCl} curves for ice in the n_{HCl} range between 10^{-7} and 10^{-3} M. The curves illustrate variation of characteristics of current maxima as functions of n_{HCl}. There is a weak dependence of the characteristic parameters of peaks 1 and 2 on the material of the electrodes (stainless steel, aluminium, and copper) (Fig. 11). Figures 9 and 12 present TSC temperatures of peaks 1 and 2 found experimentally, their maximal values and charges $Q_{1,2}$ depending on the HCl

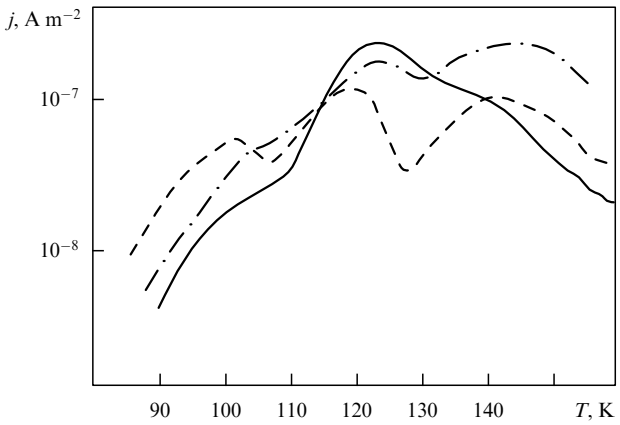

Figure 11. TSDC density as a function of temperature in HCl-doped ice ($n_{HCl} = 1.7 \times 10^{-7}$ M) with stainless steel (dashed line), copper (dot-and-dash line), and aluminium (solid line) electrodes ($E_p = 10^5$ V m^{-1}, $T_p = 240$ K, $t_p = 15$ min, and $c = 4 \times 10^{-2}$ K s^{-1}) [159].

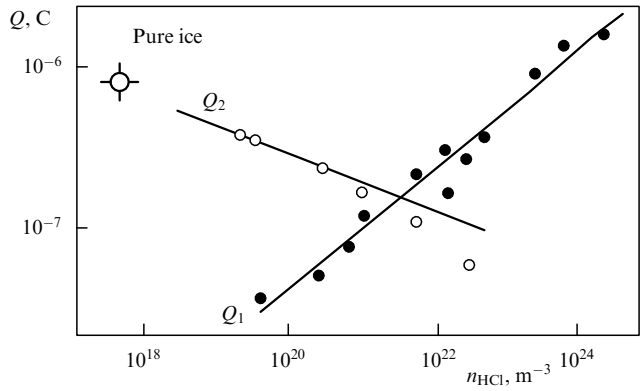

Figure 12. n_{HCl}-dependence of charges corresponding to peaks 1 and 2 [157].

concentrations [134]. U_1 increases to 0.22 eV with increasing n_{HCl} due to a better separation of the first and second relaxation processes, as well as a larger area enclosed by the TSC peak 1, in conformity with the $Q_1 \propto (n_{HCl})^{0.43}$ law, by virtue of the involvement of ion H_3O^+ defects in the relaxation process [38, 43].

The above relaxation mechanism for H_3O^+, OH^-, L-, and D-defects and H_2O molecules is not directly associated with a particular crystalline structure (e.g., ice) but is related to specific features of the hydrogen bonds and is likely to operate in any crystals where these bonds are present.

3. Electretic properties of ice

3.1 Phenomenological theory of thermally stimulated currents in ice

The TSPC density can be found by solving a closed system of equations for all partial defect fluxes. Assuming flux components to be coordinate-independent, let us introduce the following notations: e_i and σ_i are the effective charge and the ith defect conduction, respectively ($e_1 = -e_2$; $e_3 = -e_4$; $e_1 + e_3 = e$); e is the proton charge; $e_1 = 0.62e$, $e_3 = 0.38e$; $j_i(t)$ is the projection of ith flux density on the x axis, and $\Omega(t)$ and E are the corresponding projections of the configuration vector and the electric field strength on the x axis. For the configuration vector and partial fluxes, it is possible to write, following [25, 122]:

$$\frac{d\Omega}{dt} = \sum_{i=1}^{4} \eta_i j_i \,, \tag{3.1}$$

$$j_i = n_i v_i \,. \tag{3.2}$$

Here, n_i and v_i are the defect concentration and velocity respectively. The quantity η_i may be conveniently estimated using Table 2. For partial fluxes one then obtains [157]

$$j_i = (e_i E - \eta_i \Phi \Omega)\sigma_i (e_i)^{-2} \,, \tag{3.3}$$

Table 2. Partial fluxes of structural defects in single-crystalline ice.

H_3O^+	OH^-	L	D
$i = 1$	$i = 2$	$i = 3$	$i = 4$
$\eta_i = +1$	$\eta_i = -1$	$\eta_i = -1$	$\eta_i = +1$
$e_i = +e_1$	$e_i = -e_1$	$e_i = -e_3$	$e_i = +e_3$

where $\Phi = 3.85kTr_\infty$ [71], $r_\infty = 2.76$A, k is the Boltzmann constant, and T is the temperature. Equations (3.1) and (3.3) give

$$\frac{\mathrm{d}\Omega}{\mathrm{d}t} = -\frac{\Omega}{\left[\Phi(\sigma_1/e_\mathrm{i}^2 + \sigma_\mathrm{B}/e_\mathrm{B}^2)\right]^{-1}} + E\left(\frac{\sigma_1}{e_\mathrm{i}} - \frac{\sigma_\mathrm{B}}{e_\mathrm{B}}\right), \qquad (3.4)$$

where $\sigma_\mathrm{i} = \sigma_1 + \sigma_2$, and $\sigma_\mathrm{B} = \sigma_3 + \sigma_4$.

The high-frequency volume conductivity equals [25, 40]

$$\sigma_\infty = \sigma_\mathrm{i} + \sigma_\mathrm{B}\,. \qquad (3.5)$$

Since polarization is absent ($\Omega|_{t=0} = 0$) at the initial moment $t = 0$, the solution of (3.4) with respect to Ω leads to

$$\frac{\Omega(t)}{E} = \exp\left[-\int_0^t \frac{\mathrm{d}t'}{\tau_\mathrm{D}(t')}\right]\int_0^t\left(\frac{\sigma_\mathrm{i}}{e_\mathrm{i}} - \frac{\sigma_\mathrm{B}}{e_\mathrm{B}}\right) \times \exp\left[-\int_0^{t'} \frac{\mathrm{d}t''}{\tau_\mathrm{D}(t'')}\right]\mathrm{d}t'\,. \qquad (3.6)$$

Taking into account four types of charge carriers, the expression for TSPC density assumes the form

$$\begin{aligned} j(t)_\mathrm{TSPC} &= \sum_{i=1}^{4} e_i j_i = E(\sigma_\mathrm{i} + \sigma_\mathrm{B}) - \Phi\Omega\left(\frac{\sigma_\mathrm{i}}{e_\mathrm{i}} - \frac{\sigma_\mathrm{B}}{e_\mathrm{B}}\right) \\ &= E(\sigma_\mathrm{i} + \sigma_\mathrm{B}) - \left(\frac{\sigma_\mathrm{i}}{e_\mathrm{i}} - \frac{\sigma_\mathrm{B}}{e_\mathrm{B}}\right)\Phi E \\ &\quad \times \exp\left[-\int_0^t \frac{\mathrm{d}t'}{\tau_\mathrm{D}(t')}\right]\int_0^t\left(\frac{\sigma_\mathrm{i}}{e_\mathrm{i}} - \frac{\sigma_\mathrm{B}}{e_\mathrm{B}}\right) \\ &\quad \times \exp\left[-\int_0^{t'} \frac{\mathrm{d}t''}{\tau_\mathrm{D}(t'')}\right]\mathrm{d}t'\,, \end{aligned} \qquad (3.7)$$

$$\begin{aligned} j_1(t) &= \frac{j(t)}{E} - (\sigma_\mathrm{i} + \sigma_\mathrm{B}) = -\frac{e_\mathrm{p}}{c\tau_\mathrm{D}}\exp\left[-\frac{1}{c}\int_{T_0}^{T}\frac{\mathrm{d}T'}{\tau_\mathrm{D}}\right] \\ &\quad \times \int_{T_0}^{T}\left(\frac{\sigma_\mathrm{i}}{e_\mathrm{i}} - \frac{\sigma_\mathrm{B}}{e_\mathrm{B}}\right)\exp\left[\frac{1}{c}\int_{T_0}^{T'}\frac{\mathrm{d}T''}{\tau_\mathrm{D}}\right]\mathrm{d}T'\,. \end{aligned} \qquad (3.8)$$

The following notations are used in (3.7) and (3.8): $c = \mathrm{d}T/\mathrm{d}t$ is the heating rate, and

$$\frac{1}{\tau_\mathrm{D}} = \Phi\left(\frac{\sigma_\mathrm{i}}{e_\mathrm{i}^2} + \frac{\sigma_\mathrm{B}}{e_\mathrm{B}^2}\right), \quad e_\mathrm{p} = \left(\frac{\sigma_\mathrm{i}}{e_\mathrm{i}} - \frac{\sigma_\mathrm{B}}{e_\mathrm{B}}\right)\left(\frac{\sigma_\mathrm{i}}{e_\mathrm{i}^2} + \frac{\sigma_\mathrm{B}}{e_\mathrm{B}^2}\right)^{-1}.$$

Let us now consider the system of equations for TSDC density in a crystalline ice sample with ohmic electrodes:

$$\left.\begin{aligned} &\frac{\mathrm{d}\Omega}{\mathrm{d}t} = \sum_{i=1}^{4}\eta_i j_i\,, \\ &j_i = \frac{\sigma_i}{e_1^2}(e_i E - \eta_i\Phi\Omega)\,,\ E = 0\,, \end{aligned}\right\} \qquad (3.9)$$

$$\left.\begin{aligned} &\frac{\mathrm{d}\Omega}{\mathrm{d}t} = -\frac{\Omega}{\tau_\mathrm{D}(t)}\,, \\ &\Omega|_{t=0} = \Omega_0\,. \end{aligned}\right\} \qquad (3.10)$$

The solution of (3.10) yields

$$\Omega(t) = \Omega_0\exp\left[-\int_0^t\frac{\mathrm{d}t'}{\tau_\mathrm{D}(t')}\right]. \qquad (3.11)$$

Taking into account (3.10), the TSDC density is written as follows

$$\begin{aligned} j_\mathrm{TSDC}(T) &= \sum_{i=1}^{4} e_i j_i = -\sum_{i=1}^{4}\frac{\sigma_i\eta_i\Phi\Omega(t)}{e_i} \\ &= -\frac{\Omega_0 e_\mathrm{p}}{\tau_\mathrm{D}}\exp\left[-\frac{1}{c}\int_{T_0}^{T}\frac{\mathrm{d}T'}{\tau_\mathrm{D}}\right]. \end{aligned} \qquad (3.12)$$

The theoretical dependence described by (3.8) is shown in Fig. 13. The curve exhibits TSC minima following the passage of positive currents. There is a perfect coincidence of TSPC curves both taking into account static conduction and disregarding it. A minimum of negative current is apparent at around 130 K. The calculated and experimental TSPC density curves show maxima and minima at the same temperatures ($T \approx 110$ and 125 K). The parameters of the relaxators used for the computation are close to real ones; some of them were obtained in the experiment.

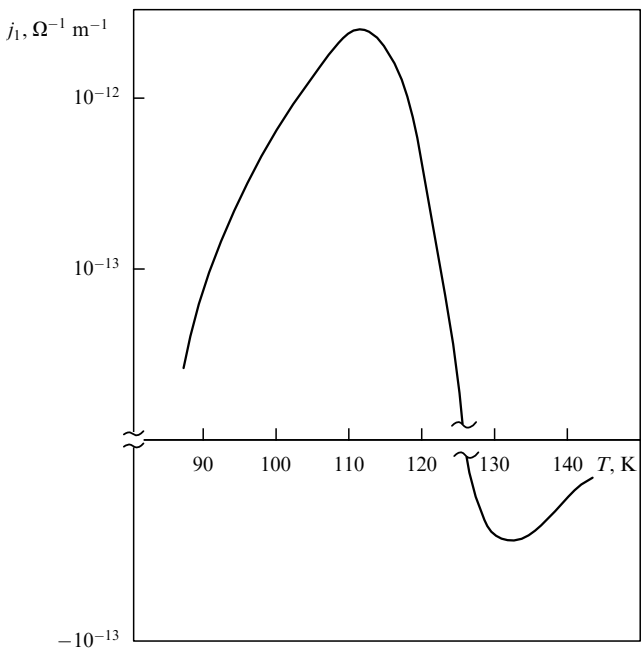

Figure 13. Theoretical dependence of j_1 (T) calculated via (3.8) [157, 159].

Therefore, there is theoretical evidence that negative TSCs in ice are due to the relaxation of four types of ion (H_3O^+, OH^-) and orientation (L, D) defects and reflect ice properties related to proton relaxation.

3.2 Thermally stimulated negative currents in ice

Negative TSDCs in pure ice were first observed in [6] and attributed to the homocharge formed and near-electrode phenomena. In early works, they were not related to intrinsic ice properties.

One of the pioneering studies on the depolarization TSC in ice was carried out by Engelhardt and Riehl [147, 149]. Johari and Jones [60–62] reviewed a wealth of TSC data for ice and concluded that two facts may be considered established with confidence: firstly, that the TSC spectrum is multicomponent, and, secondly, that depolarization currents correspond to the discharge of a heterocharged electret.

Precision measurements of ice's TSDC became possible using carefully prepared standard samples of chemically pure didistilled and degasified water having a volume electric conductivity of less than 5×10^{-5} Ohm^{-1} cm^{-1} [158].

The theoretical description of TSDC and TSPC spectra in ice samples with ohmic electrodes allows for the conclusion that TSDC and TSPC can change sign upon discharge of a homocharged electret from ice. It is convenient to begin experimental verification of this inference with pure ice.

Figure 14 presents TSDC curves obtained after thermal purification of samples at T_j 5–6 K higher than the maximal temperature T_m, followed by rapid cooling of the sample down to T_0. Further heating for $t_j \approx 15-20$ min induced negative currents (NC). The positions of NC minima for selected TSC peaks undergoing thermal purification remained unaltered. Following thermal purification of the second and third maxima, the NC peaks were localized at 116 K and 126 K, respectively.

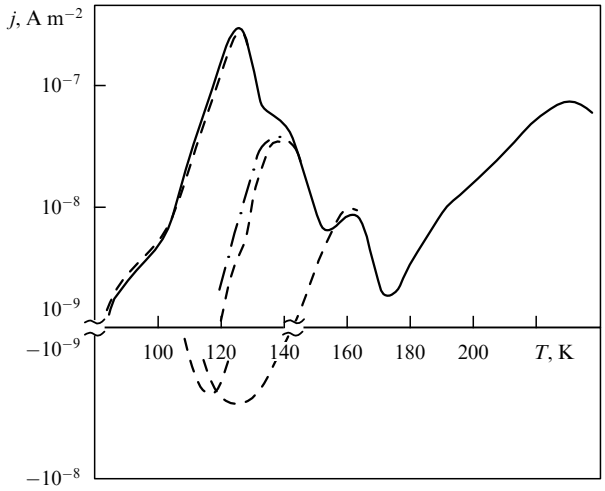

Figure 14. TSDC density as a function of temperature: TSC in pure ice (solid line); TSC in thermally purified ice (dashed line); TSC in the same sample after repeat thermal purification following thermal exposure at $T = 135$ K for $t_j = 15-20$ min [114] ($E_p = 10^5$ V m^{-1}, $T_p = 240$ K, $t_p = 15$ min, and $c = 4 \times 10^{-2}$ K s^{-1} [159]).

Results of the calculations are presented in Fig. 15 illustrating the theoretical dependences of TSDC for different concentrations of ion (H_3O^+) and orientation (L) defects derived from formula (3.12). Figure 16 shows the experimental second maxima of TSDC in pure, HCl- and NH_4OH-doped ice. Comparison of these curves demonstrates a fairly good agreement between theory and experiment. The dependence of the amplitude of peak 2 on the growing NH_4OH concentration becomes apparent as the peak shifts to the lower temperature region. In the studied NH_4OH concentration range, the charge numerically equivalent to the area enclosed by the curve of peak 2 is of the same order of magnitude as the corresponding charge in pure ice. Computer-assisted computation using the familiar Bucci and Fieschi formula (2.22) indicated that the area under peak 1 decreased as $Q \propto (n_L)^{0.43}$. The permittivity of ice at 130 K, derived from the formula

$$\varepsilon_S - \varepsilon_\infty = \frac{Q}{E_p \varepsilon_o S},$$

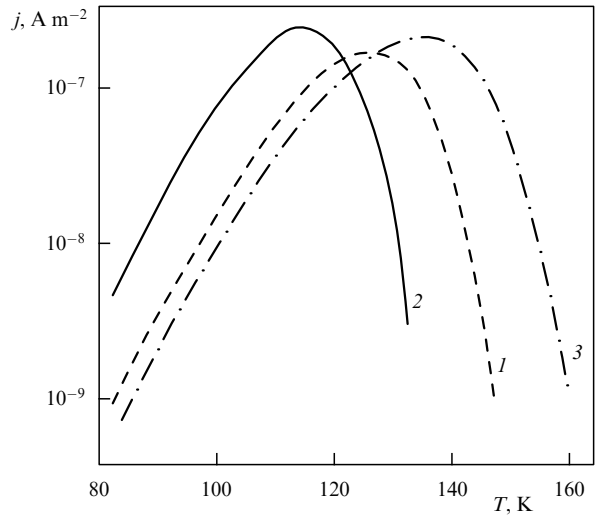

Figure 15. Theoretical dependences of TSDC density calculated using (3.12) for different concentrations of H_3O^+- and L-defects [159]: *1* — $n_{H_3O^+} = 10^{18}$ m^{-3}, $n_L = 10^{12}$ m^{-3}; *2* — $n_{H_3O^+} = 10^{19}$ m^{-3}, $n_L = 5 \times 10^{12}$ m^{-3}; *3* — $n_{H_3O^+} = 10^{17}$ m^{-3}, $n_L = 5 \times 10^{11}$ m^{-3} [114].

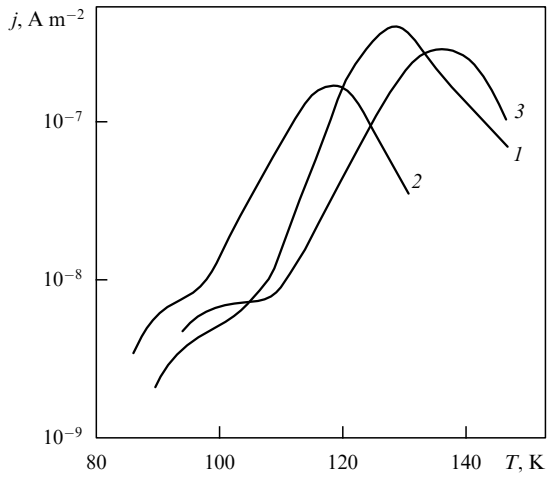

Figure 16. Experimental temperature dependences of TSDC density: *1* — pure ice; *2* — HCl-doped ice ($n_{HCl} = 4.8 \times 10^{-7}$ M); *3* — NH_4OH-doped ice ($n_{NH_4OH} = 5 \times 10^{-7}$ M) [114, 159].

and obtained from peak 1 characteristics for HCl-doped ice ($n_{HCl} = 1.2 \times 10^{-3}$ M) proved to be 300 ± 10, in agreement with the model [122]. Taken together with the dependences of Q, T_m on n_{HCl}, n_{NH_3}, this suggests the involvement of ionization (H_3O^+) and L-defects in the relaxation process at 100 K and 127 K, respectively [114].

In addition to the observed TSDC dependence, Fig. 17 shows a theoretical TSDC dependence derived from formula (3.12). There is a qualitative agreement between theory and experiment [157, 159].

Therefore, the negative currents induced by homocharge breakdown, predicted by the theory in question and found experimentally in the TSDC spectra of pure, HCl-, and NH_4OH-doped ice reflect those properties of ice which are related to changes of the configuration vector. These changes follow the breakdown of the homocharge and are responsible for the electretic state of ice. The resulting electretic charge is

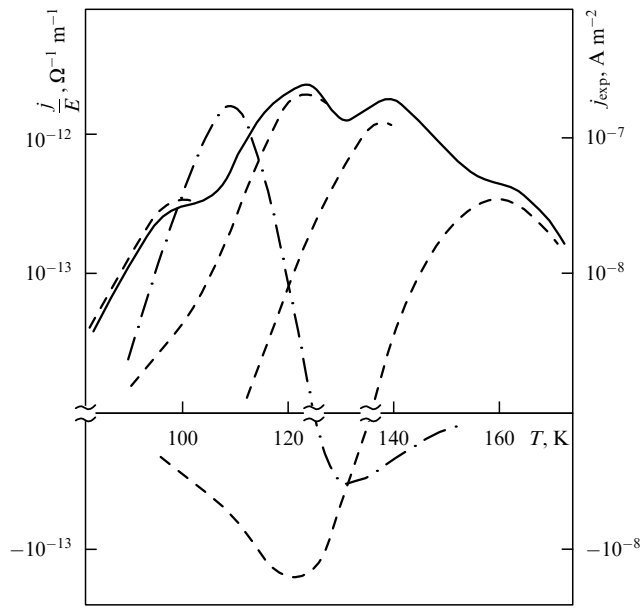

Figure 17. TSDC density as a function of temperature: experimental dependence of TSDC density for HCl-doped ice (solid curve) ($n_{\mathrm{HCl}} = 8.5\times 10^{-7}$ M); experimental dependences of TSDC density for the same sample following thermal purification (dashed curves); theoretical dependence calculated using (3.12) (dot-and-dash curve) ($E_{\mathrm{p}} = 10^5$ V m^{-1}, $T_{\mathrm{p}} = 240$ K, $t_{\mathrm{p}} = 15$ min, $c = 4\times 10^{-2}$ K s^{-1} [159]).

set up by the relaxation of protons which migrate along hydrogen bonds. It is precisely this process that determines Ω_0 as well as σ_{i} and σ_{B} in formula (3.12). The concentration of structural defects which is a function of the amount of proton-donating and proton-accepting impurities, enters to Ω_0, σ_{i}, and σ_{B} and determines both the position and the magnitude of maxima and minima in TSC spectra.

The electretic state of ice arising from thermally stimulated depolarization depends on two factors: the polarizing electric field and the configuration vector, while the electretic charge is produced by proton relaxation on hydrogen bonds.

The proton relaxation mechanisms underlying the evolution of the electretic state depend on specific features of hydrogen bonds. Therefore, they must be operative not only in ice but also in crystals containing structurally bound water.

4. Kinetic theory of polarization and depolarization of hydrogen-bonded crystals

4.1 Complex permittivity

The phenomenological theory for the field-induced accumulation of volume charge in dielectrics and semiconductors was first suggested by MacDonald [160]. Later studies [161, 162] demonstrated the marked effect of tunnelling transitions overlooked by MacDonald for dielectric relaxation at low temperatures.

We consider here transport processes for an ideal lattice taking account of neither traps nor the recombination/dissociation of charge carriers. The distance between equilibrium positions a is taken to be equal to the lattice constant. Such an approximation is not too rough for proton relaxation.

An external electric field causes the redistribution of charge carriers. Therefore, the potential relief assumed to be rectangular depends not only on the coordinate x but also on the time t. To simplify calculations, we consider the transport of a single type of charge carrier and suppose the oppositely charged carrier to have low mobility and the electrodes to be blocking.

The following system of kinetic equations ensues from the condition for the transition of relaxators between neighbouring states $i-1$, i, $i+1$ [163]:

$$\frac{\partial n_i(t)}{\partial t} = A^-_{i-1,\,i}\,n_{i-1} - (A^+_{i,\,i-1} + A^-_{i,\,i+1})n_i + A^+_{i+1,\,i}\,n_{i+1}\,, \quad (4.1)$$

where n_i is the concentration of ions in the ith state, and $A^{\pm}_{i,j}$ is the probability of ion transition from state i to state j per unit time which may be presented in the form

$$A^{\pm}_{i,j} = \frac{\nu_0}{2}\left[\exp\left(-\frac{U \pm |\Delta U_{i,j}|}{kT}\right) + B^{\pm}_{i,j}\right]. \quad (4.2)$$

In (4.2), $|\Delta U_{i,j}|$ is the change in the height of the potential barrier following transition from state i to state j:

$$|\Delta U_{i,j}| = \begin{cases} q\left[\varphi(x_i) - \varphi\left(x_i + \dfrac{a}{2}\right)\right], & i < j\,, \\ q\left[\varphi\left(x_i - \dfrac{a}{2}\right) - \varphi(x_i)\right], & i > j\,. \end{cases} \quad (4.3)$$

In (4.2) and (4.3), ν_0 is the frequency of ion oscillation in the separate potential well, U is the height of the potential barrier, q is the ion charge, k is the Boltzmann constant, φ is the electric field potential, and $B^{\pm}_{i,j}$ take into account subbarrier tunnelling transitions between neighbouring states in the quasi-classical approximation, in accordance with [161, 162]:

$$B^{\pm}_{i,j} = \frac{1}{kT}\int_{|2\Delta U_{i,j}|,0}^{U\pm|\Delta U_{i,j}|} \exp\left\{-\frac{E}{kT} - \frac{2\delta}{\hbar} \times \left[2m(U \pm |\Delta U_{i,j}| - E)\right]^{1/2}\right\} \mathrm{d}E\,, \quad (4.4)$$

$$B^-_{i,j} = \eta + \beta|\Delta U_{i,j}| - W_k\left(1 + |\Delta U_{i,j}|\frac{1}{kT}\right), \quad (4.5)$$

$$B^+_{i,j} = \eta - \beta|\Delta U_{i,j}| + W_k\left(1 - |\Delta U_{i,j}|\frac{1}{kT}\right) - \frac{2|\Delta U_{i,j}|W_{\mathrm{T}}}{kT}\,, \quad (4.6)$$

where $W_k = \exp(-U/kT)$, and $W_{\mathrm{T}} = \exp\left[-(8\delta^2 mU/\hbar^2)^{1/2}\right]$.

In (4.5) and (4.6) the following notations are introduced:

$$\eta = W_{\mathrm{T}}\left(1 + 2b\sum_{k=0}^{\infty} A_k C^{2k}\right) + W_k \sum_{k=0}^{\infty} A_k b^{k+1}\,, \quad (4.7)$$

$$\beta = \left(\frac{2m\delta^2}{\hbar^2 U}\right)^{1/2} W_{\mathrm{T}}\left[1 + \sum_{k=0}^{\infty} A_k C^{2k+1}\left(2b^{1/2} - \frac{2k+1}{c}\right)\right] + \frac{4m\delta^2}{\hbar^2} W_k \sum_{k=0}^{\infty} A_k b^k\,. \quad (4.8)$$

Here, δ is the width of the potential barrier, m is the ion mass, $b = 2\delta^2 mkT/\hbar^2$, $c = \sqrt{U/kT} - \sqrt{b}$, and $A_k = 2^k(-1)^k/(2k+1)!!$.

It appears appropriate to transform the finite difference equation (4.1) to an equation of the Fokker–Planck type. Using (4.2), (4.3) and (4.5), confining ourselves to the linear

approximation in the expansion of potentials $\varphi(x_i \pm a/2)$ in powers of $a/2$, and taking into consideration that $E = -\partial\varphi/\partial x$, we find [163]

$$\frac{\partial n}{\partial t} = D\,\frac{\partial^2 n}{\partial x^2} - \mu\frac{\partial(En)}{\partial x}\,. \tag{4.9}$$

In (4.9), the diffusion coefficient (D) and mobility (μ) have the form

$$D = \frac{v_0 a^2 \eta}{2}\,, \quad \mu = \frac{v_0 a^2 q}{2}\left(\beta + \frac{W_{\text{T}}}{kT}\right). \tag{4.10}$$

The kinetic equation (4.9) needs to be solved together with the Poisson equation

$$\frac{\partial E}{\partial x} = \frac{q}{\varepsilon\varepsilon_0}\,(n - n_0) \tag{4.11}$$

under the boundary conditions

$$\left.\frac{\partial n}{\partial x}\right|_{x=0,\,d} = \left.\frac{\mu}{D}\,nE\right|_{x=0,\,d}, \quad \int_0^d E\,\mathrm{d}x = U_0\exp(\mathrm{i}\omega t)\,, \tag{4.12}$$

where U_o is the amplitude of the applied external voltage, d is the dielectric thickness, ω is the angular frequency of the external electric field, and n_0 is the equilibrium ion concentration.

The initial condition has the form

$$n(x, 0) = n_0\,. \tag{4.13}$$

By expressing x, t, and E through the dimensionless quantities

$$\xi = \frac{x}{a}\,, \quad \tau = \frac{Dt}{a^2}\,, \quad z = \frac{E}{E_0} \tag{4.14}$$

and introducing the notations

$$\rho = n - n_0\,, \quad \gamma = \frac{\mu a E_0}{D}\,, \quad \psi = \frac{aq}{\varepsilon\varepsilon_0 E_0}\,, \quad \Theta = \psi\gamma n_0\,, \tag{4.15}$$

the system of equations (4.9) and (4.11) can be rewritten, in view of the boundary and initial conditions (4.12) and (4.13), in a modified form

$$\frac{\partial\rho}{\partial\tau} = \frac{\partial^2\rho}{\partial\xi^2} - \gamma\frac{\partial(\rho z)}{\partial\xi} - \Theta\rho\,, \quad \frac{\mathrm{d}z}{\mathrm{d}\xi} = \psi\rho\,,$$

$$\left.\frac{\partial\rho}{\partial\xi}\right|_{\xi=0,\,d/a} = \gamma(n_0 + \rho)z\Big|_{\xi=0,\,d/a}\,,$$

$$\int_0^{d/a} z\,\mathrm{d}\xi = \frac{d}{a}\exp\frac{\mathrm{i}\omega\tau a^2}{D}\,, \quad \rho(\xi, 0) = 0\,. \tag{4.16}$$

The nonlinear system of equations (4.16) has no exact solution. However, it is not infrequent that $\gamma < 1$; in this case, z and ρ can be expanded in power series of γ:

$$z = \sum_{n=0}^{\infty} z_n\gamma^n\,, \qquad \rho = \sum_{n=1}^{\infty}\rho_n\gamma^n\,. \tag{4.17}$$

As a rule, the tangent of the dielectric loss angle is measured using low intensities of the electric field. Therefore, it will suffice to be confined in (4.17) to the terms linear in γ:

$$z = z_0 + z_1\gamma\,, \quad \rho = \rho_1\gamma\,. \tag{4.18}$$

The substitution of (4.18) into (4.16) yields

$$\frac{\partial\rho_1}{\partial\tau} = \frac{\partial^2\rho_1}{\partial\xi^2} - \Theta\rho_1\,, \quad \frac{\partial z_0}{\partial\xi} = 0\,,$$

$$\left.\frac{\partial\rho_1}{\partial\xi}\right|_{\xi=0,\,d/a} = z_0 n_0\,, \quad \rho_1(\xi, 0) = 0\,,$$

$$\int_0^{d/a} z_0\,\mathrm{d}\xi = \frac{d}{a}\exp\frac{\mathrm{i}\omega\tau a^2}{D}\,. \tag{4.19}$$

It follows from (4.19) that $z_0 = \exp(\mathrm{i}\omega\tau a^2/D)$. Eqn (4.19) is solved using a Laplace transform. The solution of (4.19) in the 'image' is [163]

$$\rho_1(p) = \frac{n_0}{p - \mathrm{i}\omega a^2/D}\,\frac{1}{\sqrt{p+\Theta}} \times \frac{\cosh\left(\sqrt{p+\Theta}\,\xi\right) - \cosh\left[\sqrt{p+\Theta}(\xi - d/a)\right]}{\sinh\left(\sqrt{p+\Theta}\,d/a\right)}\,. \tag{4.20}$$

Passing to the original in variables x and t in expression (4.20) and taking into account (4.15) and (4.18), we find

$$\rho(x, t) = -\frac{4\mu n_0 E_0}{d}\sum_{k=1}^{\infty}\frac{\sin^2(\pi k/2)\cos(\pi k x/d)}{1 + \mathrm{i}\omega\tau_k} \times \left[\exp(\mathrm{i}\omega t) - \exp\left(-\frac{t}{\tau_k}\right)\right]. \tag{4.21}$$

It follows from (4.21) that the distribution of charge carriers is described by the sum of spatial harmonics, with only odd harmonics making a nonzero contribution, each characterized by its own relaxation time τ_k:

$$\frac{1}{\tau_k} = \frac{1}{\tau_{\text{M}}} + \frac{1}{\tau_{\text{d}k}}\,, \tag{4.22}$$

where $\tau_{\text{M}} = \varepsilon\varepsilon_0/\mu q n_0$ is the Maxwellian relaxation time, and $\tau_{\text{d}k} = d^2/\pi^2 k^2 D$ is the relaxation time due to diffusion.

It appears from (4.22) that the following situations should be distinguished: Maxwellian relaxation at $\tau_{\text{d}k} \gg \tau_{\text{M}}$, diffusive relaxation at $\tau_{\text{M}} \gg \tau_{\text{d}k}$, and an intermediate case at $\tau_{\text{M}} \sim \tau_{\text{d}k}$. Similar to what was found in Refs [161, 162], tunnelling of relaxators leads to non-Debye dispersion below the characteristic temperature [163]

$$T_S = \frac{1}{2k}\left(\frac{\hbar^2 U}{2\delta^2 m}\right)^{1/2}. \tag{4.23}$$

The relaxation time decreases with increasing harmonic number; hence, there is a periodic solution at $t \gg \tau_1$ [163]:

$$\rho(x, t) = -\frac{4\mu n_0 E_0}{d}\sum_{k=1}^{\infty}\frac{\sin^2(\pi k/2)\cos(\pi k x/d)}{1 + \mathrm{i}\omega\tau_k}\exp(\mathrm{i}\omega t)\,. \tag{4.24}$$

Using (4.24) allows the polarization intensity averaged over the coordinate to be computed:

$$P(t) = \frac{8\mu n_0 E_0}{\pi^2}\sum_{k=1}^{\infty}\frac{\sin^2(\pi k/2)\tau_k}{k^2(1 + \mathrm{i}\omega\tau_k)}\exp(\mathrm{i}\omega t)\,. \tag{4.25}$$

The electric field energy scattered in a unit volume during a period is derived from the expression

$$Q = \overline{\operatorname{Re} E \operatorname{Re} \frac{\partial P}{\partial t}}. \tag{4.26}$$

The bar in (4.26) defines averaging over time.

Let us now calculate the imaginary part of the permittivity

$$\varepsilon'' = \frac{2}{\omega E_0^2} \overline{\operatorname{Re} E \operatorname{Re} \frac{\partial P}{\partial t}}. \tag{4.27}$$

By substituting (4.25) into (4.27) and taking into account that $\operatorname{Re} E = E_0 \cos \omega t$, we have

$$\varepsilon'' = \frac{8\mu q n_0}{\pi^2} \sum_{k=1}^{\infty} \frac{\tau_k}{k^2} \frac{\sin^2(\pi k/2)\omega\tau_k}{1+\omega^2\tau_k^2}. \tag{4.28}$$

The real part of the permittivity is determined from the Kramers – Kronig relationship

$$\varepsilon' = \varepsilon_\infty + \frac{8\mu q n_0}{\pi^2} \sum_{k=1}^{\infty} \frac{\tau_k}{k^2} \frac{\sin^2(\pi k/2)}{1+\omega^2\tau_k^2}. \tag{4.29}$$

4.2 Thermally stimulated depolarization currents

The TSDC is measured under specific experimental conditions, that is after polarization of the 'frozen' crystalline state is completed accounting for the equilibrium number and distribution of relaxators in the crystal. In this case, the concentration of structural defects may be determined using the Boltzmann distribution which greatly simplifies the solution of the system of kinetic equations above [164].

Let us represent the model of a crystal as a system of m sufficiently deep wells (layers) [2]. The concentration of charged defects for the ith state found from the Boltzmann distribution is

$$n_i^0 = n_0 \exp \frac{q\varphi_i}{\Theta_\mathrm{p}}, \quad n_{i-1}^0 = n_0 \exp \frac{q\varphi_{i-1}}{\Theta_\mathrm{p}}, \tag{4.30}$$

whence

$$n_i^0 = n_{i-1}^0 \exp \frac{q\Delta\varphi_{i,i-1}}{\Theta_\mathrm{p}}, \tag{4.31}$$

where $\Delta\varphi_{i,i-1}$ may be regarded as the difference of potentials between equipotential layers i and $i-1$, q is the effective charge, Θ_p is the absolute polarization temperature: $\Theta_\mathrm{p} = kT_\mathrm{p}$.

Neglecting the intrinsic field of relaxators, expression (4.31) can be transformed to

$$n_i^0 = n_{i-1}^0 \exp \frac{qaE_\mathrm{p}}{\Theta_\mathrm{p}},$$

or

$$n_i^0 = n_1^0 \alpha^{2(i-1)}. \tag{4.32}$$

In (4.32), $\alpha = \exp(qaE_\mathrm{p}/2\Theta_\mathrm{p})$ and a is the lattice constant.

According to the charge conservation law

$$\sum_{i=1}^{m} n_i^0 = n_1^0\alpha^0 + n_1^0\alpha^2 + \ldots + n_1^0\alpha^{2(m-1)}. \tag{4.33}$$

Let us multiply both parts of Eqn (4.33) by α^2 and subtract (4.33) from the product. Then we arrive at

$$\alpha^2 \sum_{i=1}^{m} n_i^0 - \sum_{i=1}^{m} n_i^0 = n_i^0\alpha^{2m} - n_i^0.$$

Therefore,

$$\sum_{i=1}^{m} n_i^0 = \frac{n_1^0(\alpha^{2m}-1)}{\alpha^2-1}.$$

Since

$$n = \sum_{i=1}^{m} n_i^0,$$

and taking into account (4.32), it follows

$$n = \frac{n_i(\alpha^{2m}-1)}{\alpha^{2(i-1)}(\alpha^2-1)}.$$

Hence, the initial condition takes the form

$$n_i^0 = \frac{n(\alpha^2-1)}{\alpha^{2m}-1}\,\alpha^{2(i-1)}, \tag{4.34}$$

where n is the mean concentration of defects in the crystal.

When the contact with electrodes is good, the boundary conditions have the form $n_0 = n_{m+1} = 0$, and depolarization is described by the above system of coupled nonlinear differential equations (4.1) which describe transitions of charged relaxators:

$$\begin{aligned}
&\frac{\mathrm{d}n_1}{\mathrm{d}\Theta}\beta = -\lambda n_1 + \lambda n_2, \\
&\ldots\ldots\ldots\ldots\ldots\ldots\ldots\ldots \\
&\frac{\mathrm{d}n_i}{\mathrm{d}\Theta}\beta = \lambda n_{i-1} - 2\lambda n_i + \lambda n_{i+1}, \\
&\ldots\ldots\ldots\ldots\ldots\ldots\ldots\ldots \\
&\frac{\mathrm{d}n_m}{\mathrm{d}\Theta}\beta = \lambda n_{m-1} - \lambda n_m.
\end{aligned} \tag{4.35}$$

According to [3, 2], one obtains

$$\lambda = f\nu \exp\left(-\frac{U}{\Theta}\right), \tag{4.36}$$

$$f = \frac{v}{2av - v}. \tag{4.37}$$

Here, v is the velocity of sound in a crystal, ν is the natural frequency of particle oscillations, U is the activation energy for the movement of the charge between the layers, and $\beta = \mathrm{d}\Theta/\mathrm{d}t$.

The rate of transition to equilibrium state is determined by the difference between particle concentrations in layers i. There is no sense in transforming the system (4.35) to the Fokker – Planck equation [164]. Let us take advantage of the approximation from Refs [2, 3], where it is assumed that

$$n_i = \frac{n}{m} - \frac{n_{i+1} - n_i}{2}. \tag{4.38}$$

Using the expansion

$$n_{i+1} = \sum_{k=1}^{m-1} A_k(\Theta) S_i^k, \tag{4.39}$$

in which

$$S_i^k = \sqrt{\frac{2}{m}} \sin\left(\frac{k\pi i}{m} + \pi i\right), \tag{4.40}$$

the system of equations (4.35) can be presented in the form

$$\begin{aligned}\frac{\mathrm{d}A_k}{\mathrm{d}\Theta} \sin\left(\frac{k\pi(i-1)}{m} + \pi(i-1)\right)\sqrt{\frac{2}{m}}\beta &= \lambda A_k \sqrt{\frac{2}{m}} \\ &\times \sin\left(\frac{k\pi(i-2)}{m} + \pi(i-2)\right) - 2\lambda A_k \sqrt{\frac{2}{m}} \\ &\times \sin\left(\frac{k\pi(i-1)}{m} + \pi(i-1)\right) + \lambda A_k \sqrt{\frac{2}{m}} \\ &\times \sin\left(\frac{k\pi i}{m} + \pi i\right). \end{aligned} \tag{4.41}$$

By combining the first and the third terms in the right-hand side of Eqn (4.41), we find that

$$\frac{\mathrm{d}A_k}{\mathrm{d}\Theta} = -\frac{4\lambda}{\beta} A_k \cos^2\left(\frac{k\pi}{2m}\right). \tag{4.42}$$

The latter equation may be used to determine parameters A_k:

$$A_k = a_k \exp\left[-\int_{\Theta_0}^{\Theta} \frac{4\lambda}{\beta} \cos^2\left(\frac{k\pi}{2m}\right) \mathrm{d}\Theta\right]. \tag{4.43}$$

Let us substitute (4.39) and (4.40) into (4.38). After the transformation taking into account (4.43), the concentration of relaxators in the ith layer is

$$\begin{aligned} n_i = \frac{n}{m} - \frac{1}{2}\sum_{k=1}^{m-1} a_k (S_i^k - S_{i-1}^k) \\ \times \exp\left[-\int_{\Theta_0}^{\Theta} \frac{4\lambda}{\beta} \cos^2\left(\frac{k\pi}{2m}\right) \mathrm{d}\Theta\right]. \end{aligned} \tag{4.44}$$

Equation (4.44) suggests the independence of relaxation modes characterized by the wave numbers k. The coefficients a_k may be calculated by using the initial conditions (4.34) and normalization of eigenfunctions (4.39) and (4.38), from which it follows that

$$\sum_{k=1}^{m-1} S_i^{k_0}(S_{i+1}^k - S_{i-1}^k) = -2\cos\left(\frac{k\pi}{2m}\right)\delta_{kk_0}, \tag{4.45}$$

where

$$\delta_{kk_0} = \begin{cases} 1, & k = k_0, \\ 0, & k \neq k_0. \end{cases} \tag{4.46}$$

Let us write (4.45) for n_{i+1} and n_i at $\Theta = \Theta_0$. The subsequent transformation yields

$$\sum_{i=1}^{m-1} S_i^{k_0}(n_{i+1}^0 - n_i^0) = \frac{1}{2} a_k \sum_{k=1}^{m-1}\sum_{i=1}^{m-1} S_i^{k_0}(S_{i+1}^k + S_{i-1}^k - 2S_i^k), \tag{4.47}$$

where

$$\sum_{i=1}^{m-1} S_i^{k_0} S_i^k = \frac{2}{m}\sum_{i=1}^{m-1} \sin\left(\frac{k_0\pi i}{m} + \pi i\right) \sin\left(\frac{k\pi i}{m} + \pi i\right).$$

If the product of sines is substituted by the difference of cosines, then

$$\sum_{i=1}^{m-1} S_i^{k_0} S_i^k = \begin{cases} 1, & k = k_0, \\ 0, & k \neq k_0. \end{cases}$$

Taking into consideration (4.34), (4.45), and (4.46) leads to

$$a_k = \frac{n}{2} \frac{(\alpha^2 - 1)^2}{(\alpha^{2m} - 1)\cos^2(k\pi/2m)} \sum_{i=1}^{m-1} S_i^k \alpha^{2(i-1)}. \tag{4.48}$$

Let us substitute (4.40) into (4.48) taking into account the expression for α. Then, the summation of (4.48) over i yields

$$\begin{aligned} a_k = \sqrt{\frac{2}{m}} \frac{(\alpha^2 - 1)^2}{\alpha^{2m} - 1}\left[1 - (-1)^{m+k}\alpha^{2m}\right] \\ \times \frac{n\tan(k\pi/2m)}{(\alpha^2 - 1)^2 + 4\alpha^2\cos^2(k\pi/2m)}. \end{aligned} \tag{4.49}$$

As a result, the concentration of charged relaxators is

$$\begin{aligned} n_i = \frac{n}{m} - \frac{n}{m}\frac{(\alpha^2 - 1)^2}{\alpha^{2m} - 1}\sum_{i=1}^{m-1}\left[1 - (-1)^{m+k}\alpha^{2m}\right] \\ \times \frac{\tan(k\pi/2m)}{(\alpha^2 - 1)^2 + 4\alpha^2\cos^2(k\pi/2m)} \\ \times \left[\sin\left(\frac{k\pi i}{m} + \pi i\right) - \sin\left(\frac{k\pi(i-1)}{m} + \pi(i-1)\right)\right] \\ \times \exp\left[-\int_{\Theta_0}^{\Theta} \frac{4\lambda}{\beta}\cos^2\left(\frac{k\pi}{2m}\right)\mathrm{d}\Theta\right]. \end{aligned} \tag{4.50}$$

To summarize, the rate of charge redistribution between different layers depends on the deviation of internal parameters from equilibrium values. This accounts for the reciprocal motion of charged relaxators inside the layers.

Crystal polarization intensity is defined by the formula

$$P = \frac{aq}{2}\sum_{i=1}^{m}(m - 2i + 1)(n_{m-i+1} - n_i). \tag{4.51}$$

The TSC density being $j = \mathrm{d}P/\mathrm{d}t = (\mathrm{d}P/\mathrm{d}\Theta)\beta$, the substitution of (4.50) into (4.51) leads to

$$\begin{aligned} j = -\frac{8aqn}{m}\Bigg\{\lambda(\alpha^2 - 1)\frac{\alpha^{2m} + 1}{\alpha^{2m} - 1} \\ \times \sum_{k=1}^{(m-1)/2} \frac{\cos^2(\pi/2m)(m - 2k + 1)}{(\alpha^2 - 1)^2 + 4\alpha^2\cos^2(\pi/2m)(m - 2k + 1)} \\ \times \tan^2\left(\frac{\pi}{2m}\right)(m - 2k + 1) \\ \times \exp\left[-\int_{\Theta_0}^{\Theta} \frac{4\lambda}{\beta}\cos^2\left(\frac{\pi}{2m}\right)(m - 2k + 1)\,\mathrm{d}\Theta\right]\Bigg\}. \end{aligned} \tag{4.52}$$

The minus sign indicates that the current density vector and the intensity of the electric field have opposite directions.

In our case, $k \ll m$, $m \gg 1$.

By expanding trigonometric functions in a series, it is possible to simplify (4.52) and obtain a formula which facilitates calculations using a computer:

$$j = -\frac{8aqn}{m}\lambda \sum_{k=1}^{(m-1)/2} \exp\left(-\int_{T_0}^{T} \frac{\pi^2\lambda(2k - 1)^2}{\beta m^2}\,\mathrm{d}T\right), \tag{4.53}$$

where $k = 1, 2, 3, \ldots$, and $\beta = \mathrm{d}T/\mathrm{d}t$.

5. Proton relaxation in crystalline hydrates and micas

5.1 Relaxing structural defects. TSDC spectra in hydrogen-bonded crystals

In complex crystalline structures containing water and OH^- radicals (crystalline hydrates, micas), the assembly of relaxators includes water molecules, besides Bjerrum defects. Other feasible relaxators are bonded by strong chemical forces and may show up only when the temperature is sufficiently low and tunnelling transitions are competitive.

Figures 18 – 20 present the TSDC density spectra of talc, phlogopite, and muscovite (common mica) at different T_p and E_p. For the first six maxima, $j_{max} = f(E_p)$ and $j_{max} = f(T_p)$ (Fig. 21) correspond to dipole polarization [10]. The TSDC density in peak 7 is not proportional to E_p. With decreasing T_p, regardless of the annealing temperature T_{an}, this peak tends to shift to the lower temperature region as far as to overlap peak 6. At a fixed polarization temperature T_p, the position of peak 7 depends on the sample annealing temperature. It is therefore suggested that this peak is due to volume charge relaxation.

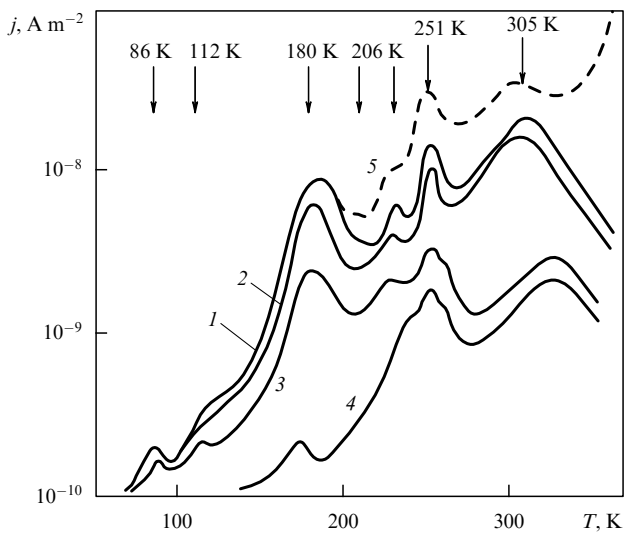

Figure 18. Temperature dependence of the TSDC density for talc at different annealing temperatures and $E_p = 2 \times 10^5$ V m^{-1}, $T_p = 300$ K: *1* — no annealing; *2* — $T_{an} = 473$ K; *3* — $T_{an} = 1023$ K; *4* — $T_{an} = 1323$ K, TSPC in the absence of annealing at $E_p = 2 \times 10^5$ V m^{-1} and $c = 0.1$ K s^{-1} [166].

The TSDC maxima for talc were recorded at 86, 112, 180, 206, 230, 251, and 305 K. The TSDC peaks for gypsum ($CaSO_4 \cdot 2H_2O$), blue vitriol ($CuSO_4 \cdot 5H_2O$) [165, 166], and muscovite ($KAl_2[AlSi_3O_{10}](OH)_2$) were apparent at approximately the same temperature, while peak 7 for phlogopite turned out to be markedly shifted (100, 130, 178, 206, 235, 260, and 405 K; see Fig. 21). Peaks 1 and 2 were very low and showed up only when the intensity of the polarizing field was in excess of 10^5 V m^{-1}.

Thermal treatment of water-containing ionic structures such as mica and talc may be an effective tool for the assessment of the role of dipoles in the relaxation process, unlike that of ice where all attempts to activate water molecules have failed because of decomposition of the crystals.

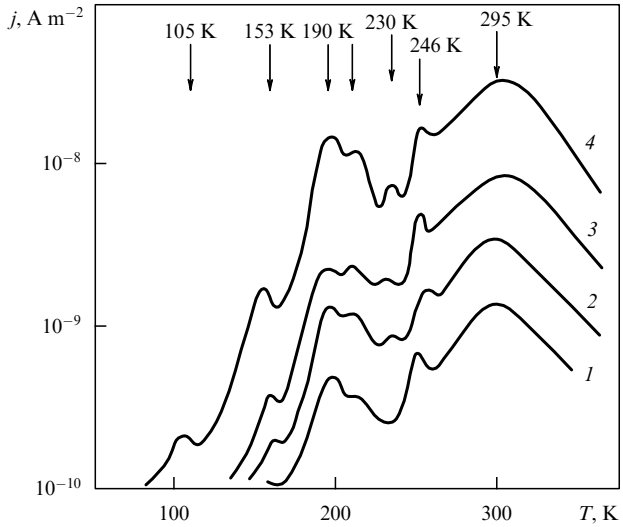

Figure 19. TSDC density as a function of temperature and E_p in muscovite at $T_p = 300$ K and $t_p = 15$ min: *1* — $E_p = 2 \times 10^5$ V m^{-1}; *2* — $E_p = 5 \times 10^5$ V m^{-1}; *3* — $E_p = 10^6$ V m^{-1}; *4* — $E_p = 5 \times 10^6$ V m^{-1} and $c = 0.1$ K s^{-1} [166, 178].

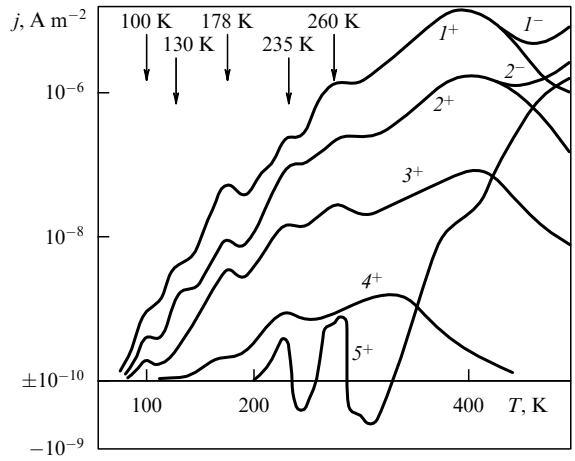

Figure 20. TSDC density spectrum in phlogopite for $E_p = 10^6$ V m^{-1}, $T_p = 373$ K, and $d = 30$ μm: 1^+, 1^- — natural; 2^+, 2^- — $T_{an} = 873$ K; 3^+ — $T_{an} = 1073$ K; 4^+ — $T_{an} = 1373$ K; *5* — TDC density spectrum. The sign alongside the digit defines the polarity of the sample [179].

Another way to act upon relaxators is by doping crystals with proton-donating or proton-accepting impurities.

In order to understand the nature of the peaks related to the relaxation of water molecules, the samples were sequentially annealed in the temperature range from 473 to 1373 K. At $T_{an} = 473$ K, most crystals lost water adsorbed at separated layers which resulted in a 10 – 100-fold reduction of peak 4. Desorption occurred at $T_{an} = 570$ K [167].

Early structural changes in the talc crystal lattice appear after annealing above 850 K due to the release of crystallization water molecules [168]. This process terminates at $T_{an} = 1323$ K. It starts at $T_{an} = 333$ K for calcium sulfate, and at 573 K for copper sulfate. Just at these temperatures, peak 3 subsides and disappears (see Fig. 18). In phlogopite, this maximum disappears at $T_{an} = 1037$ K [168, 169] because of the presence of water lenses and gas-liquid inclusions (see Fig. 20). These inclusions also affect the height dependence of peak 3 on the sample thickness (Fig. 22). The estimated

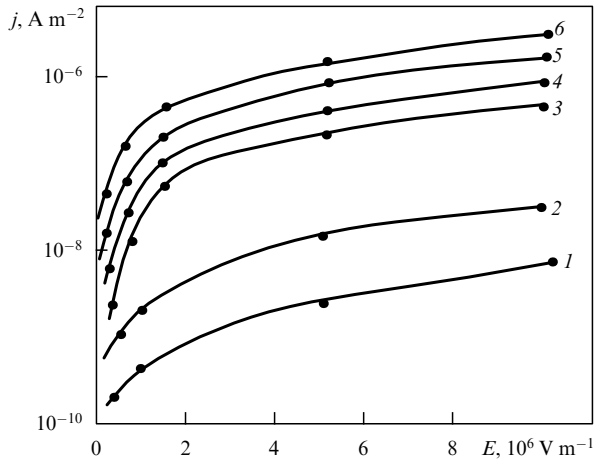

Figure 21. TSDC density as a function of E_p in phlogopite for different maxima: *1* — $T_m = 100$ K; *2* — $T_m = 130$ K; *3* — $T_m = 178$ K; *4* — $T_m = 206$ K; *5* — $T_m = 235$ K; *6* — $T_m = 257$ K [179].

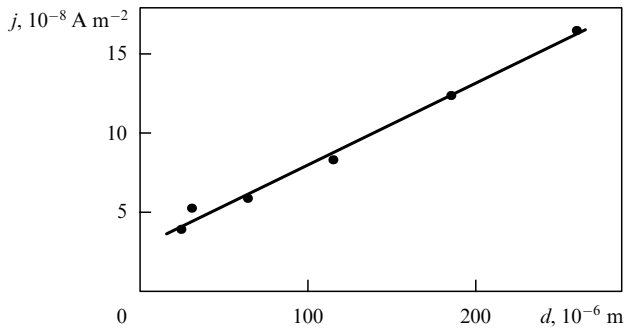

Figure 22. TSDC density as a function of sample thickness for the third maximum in the phlogopite spectrum at $E_p = 10^6$ V m^{-1}, $T_p = 300$ K [179].

energy of water dipole attraction to the lower packet of silicooxygen tetrahedrons in mica is 0.23 eV [168]. Within experimental error, this value is close to the activation energy of crystallization water molecules (peak 3) (Table 3).

Table 3. Activation energies derived from a TSDC spectrum.

Peak No.	Talc		Phlogopite	
	T_m, K	U, eV	T_m, K	U, eV
1	86	0.06±0.01	100	0.05±0.01
2	112	0.09±0.02	130	0.17±0.02
3	180	0.19±0.02	178	0.25±0.03
4	206	0.25±0.03	206	0.31±0.03
5	230	0.32±0.04	235	0.40±0.04
6	251	0.41±0.04	260	0.49±0.05
7	305	0.40±0.06	405	0.35±0.05

Phlogopite crystals annealed to 1373 K appear to lose less than 30% of their constitutional hydrated oxides [168]. In this case, peak 5 (235 K) does not totally disappear. Similar effects are reported for talc, muscovite, crystalline hydrates of calcium and copper sulfate [165, 166]. The activation energies of OH^- ions derived from IR and Raman scattering spectra [168, 170] coincide, to within the error, with those for peak 5 in TSDC spectra (Table 3). This means that peak 5 is related to the relaxation of OH^- ions.

The nature of peaks 1, 2, 5, and 6 was examined by the method proposed in [171]. Doping of the samples in HCl and NH_4OH solutions of different concentrations for 60 – 100 days resulted in a shift of maxima 2 and 6 relative to the standard sample spectra. For HCl-doped crystals, it was evident a shift of peak 6 to the lower temperature range, according to (2.21), while the same peak for NH_4OH-doped crystals shifted to the higher temperature region. In the latter case, there was a prominent rise in peak 5 (Fig. 23). Similar shifts of TSC maxima are typical of doped ice crystals as well [156].

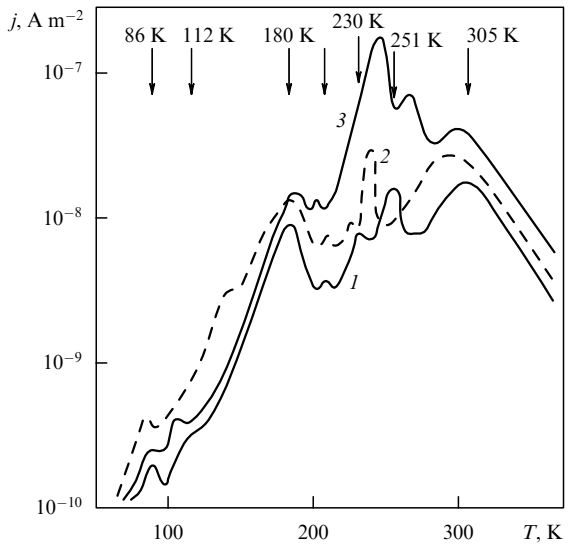

Figure 23. Effect of talc doping on TSDC spectrum: *1* — natural talc; *2* — HCl-doped talc ($n_{HCl} = 7.4$ mol l^{-1}); *3* — NH_4OH-doped talc ($n_{NH_4OH} = 9.2$ mol l^{-1}); $E_p = 2 \times 10^5$ V m^{-1}, $T_p = 300$ K [166].

It follows from the comparison of TSDC spectra and the activation energies that peak 2 in both sulfate and silicate crystalline hydrates is due to the relaxation of ion H_3O^+ defects, whereas peak 6 is related to the formation of 'vacancy + L-defect' (VL) or 'vacancy + D-defect' (VD) complexes [165]. In [172], the activation energy of VL (VD) complexes is estimated to be 0.4 – 0.5 eV, similar to our data (Table 3). Also, complexes of interstitial molecules with L- and D-defects are conceivable [173]. The types of relaxators and their modes of orientation are presented in Table 4.

5.2 Electretic properties of phlogopite

Additional studies have been carried out to account for the position and magnitude of peak 7 in phlogopite spectra.

A change in the sample polarity gave rise to a reversal of the current sigh in the spectra of thermodepolarization currents (TDC) used to study electrets [174]. The current density increased from 10^{-10} A m^{-2} at 220 K to 10^{-6} A m^{-2} at 450 – 500 K (Fig. 24). The TDC was measured in the absence of polarization and an electric field. The data obtained indicate that natural phlogopite specimens are electrets. It proved possible to prepare a thermoelectret of phlogopite plates at $T_p = 473$ K, $E_p = 10^7$ V m^{-1}, and $t_p = 2$ h in which, when short-circuited, the electretic current of about 10^{-10} A persisted for a few months at room temperature.

Table 4. TSDC maxima positions, types of relaxators, and their mechanisms of orientation in phlogopite.

Peak No.	T_m, K	Type of relaxator	Orientation mechanism
1	100	$HSiO_4^{3-}$	Proton tunnelling. Proton transition inside and between anions.
2	130	H_3O^+	Ionization. Proton transition between H_2O molecules.
3	178	H_2O (crystallization water)	Dipolar
4	206	H_2O (adsorbed at separated layers)	Dipolar
5	235	OH^-	Ionization. Proton transition between H_2O molecules.
6	260	VL (VD)	Orientational. Rotation of H_2O molecules and formation of complexes.
7	405	H_3O^+, OH^-, H^+	Interlayer polarization. Charge accumulation and dispersal. Superimposed electretic current.

The TDC resulting from decay of the electretic state was characterized by maxima, the number of which corresponded to the number of monorelaxation processes [175]. The electret charge was calculated by summing the area enclosed by TDC curves and taking into account the current sign. It turned out to be 3×10^{-7} C.

The TDC was measured not only for the thermoelectret but also after the TSDC spectrum was obtained. There occurred residual polarization in both cases. The TDC spectra exhibited seven maxima (see Fig. 24) which it proved difficult to distinguish because the thermal purification technique was found inapplicable to thermoelectrets. Nevertheless, the number of maxima gives an idea of how many relaxators underlie the electretic state.

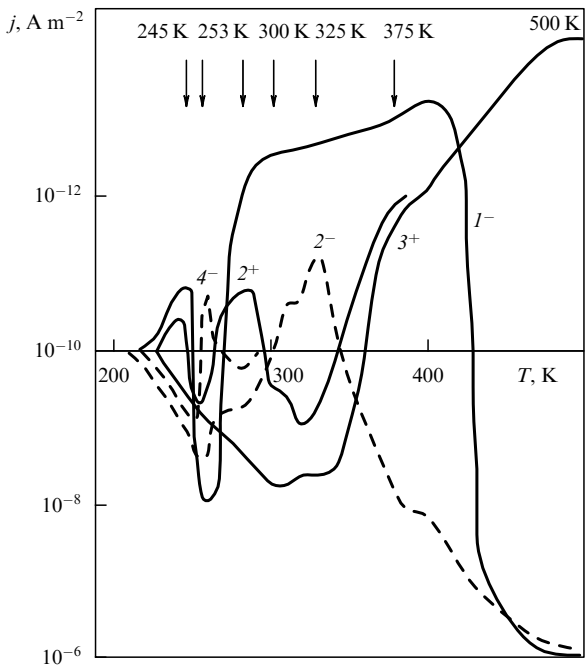

Figure 24. TDC density spectrum in phlogopite for $T_{an} = 873$ K: *1* — the early spectrum; 2^+ and 2^- — the same after 15 days; 3^+ — the same after 16 days; 4^- — $T_{an} = 1073$ K. The sign alongside the digit defines the polarity of the sample [179].

The appearance of TDCs with either sign may be attributed to the formation of the electretic state in phlogopite crystals. The presence of positive maxima is due to the heterocharge which results from freezing oriented dipoles and protons displaced along hydrogen bonds in the electric field. This picture does not contradict the Gross theory [176, 175].

The homocharge characterized by negative maxima is normally formed when ions or electrons from a metallic electrode are injected into a crystal. The heterocharge may undergo transformation to a homocharge upon neutralization of the ions shifted towards electrodes by the conduction current. During this transformation, a part of the heterocharge disappears and the number of implanted ions which have the opposite sign to that of the displaced ions, may exceed the number of bound dipoles [175, 177]. This was confirmed in our experiments (see Fig. 24). Another TDC spectrum obtained 15 days after the first also suggests the loss of a part of the heterocharge and exhibits the residual maximum at $T = 325$ K (see Fig. 24, curves 1^-, 2^-, 2^+). Further measurements also showed a single broadened negative maximum for the reversed polarity of the sample in this temperature region, which was later stabilized (curves 2^+ and 3^+).

Therefore, phlogopite crystals possess properties intrinsic in electrets, namely, a long-lived charge with a relatively short Maxwellian relaxation time, a sign inversion from hetero- to homocharge, 'external' and 'internal' residual polarizations, and opposite directions for the TDC with volume distribution of hetero- and homocharges. At a high annealing temperature, the charges are dispersed and electretic properties disappear (see Fig. 24, curve 4^-) [178, 179].

The TSDC and TDC spectra suggest that both the magnitude and the position of TSDC peak 7 are due to an electretic current. Gemant [180] and Pugett and Gubkin [175] argue that electrets may arise from substances containing polar groups, in particular, OH^- ions. It is supposed that the TDC maximum at 240 K is also dictated by relaxation with the OH^- involved (Table 4), whereas the maximum at 375 K is related to volume charge dispersal caused by the migration of H_3O^+ and OH^- ions and protons. Here, as in ice, a change in the proton subsystem state is apparent [114]. It is proton migration that is responsible for the appearance of H_3O^+ and OH^- dipoles facilitating the formation of the electretic state. There is every reason to believe that proton relaxation is a major cause of the phlogopite electretic state.

5.3 Mechanism of structural defect migration in hydrogen-bonded crystals

It was demonstrated in Ref. [166] that the electric conduction in layered crystals like those of gypsum and talc is largely due to the movement of OH^- ions at high temperatures and H_3O^+ ions at low temperatures when proton tunnelling is feasible. Dielectric relaxation is also related to proton migration as ensues from the dependence $\ln \tau = f(1/T)$ constructed based on the $\tan \delta = f(\nu, T)$ spectra in the temperature range from 77 to 350 K [165]. The structures of talc ($Mg_3[Si_4O_{10}](OH)_2$) and muscovite ($KAl_2[AlSi_3O_{10}](OH)_2$) are peculiar in that the distance between SiO_4^{4-} layers does not exceed 1.8 A, i.e. the hydrogen bridge length [181]. Therefore, as in the case of gypsum [166], there are two possibilities for the diffusion of H_3O^+ defects:

(1) migration of H_3O^+ ions along a water layer and between H_2O molecules of adjacent layers;

(2) migration of H_3O^+ ions between H_2O and SiO_4-ion layers.

A proton placed between two neighbouring water molecules can overcome the potential barrier when driven by thermal fluctuations and the applied electric field, and shift along a hydrogen bond from one water molecule to another, thus giving rise to an ion H_3O^+ defect. The concentration of such defects can be increased by introducing proton-donating impurities. The migration of a proton is mirrored in the movement of an H_3O^+ defect. A rise in the proton-donating concentration is accompanied by an enhancement of the electric conductivity (Fig. 25) in conformity with Refs [166, 182].

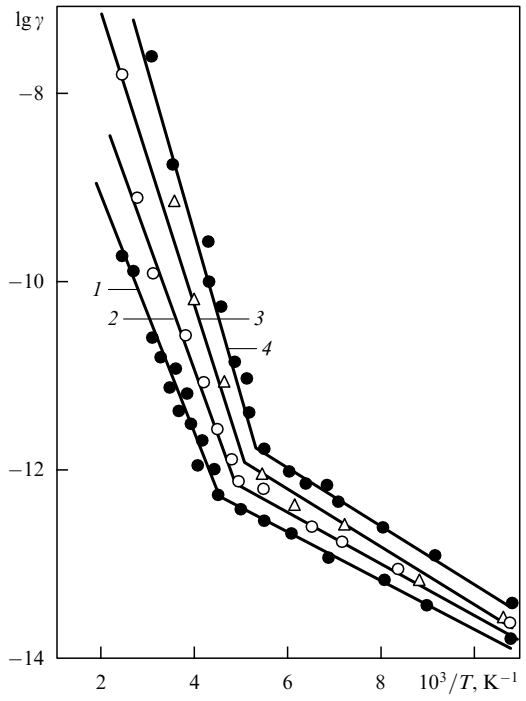

Figure 25. Volume electric conductivity in HCl-doped talc as a function of temperature: *1* — natural talc, $T_{an} = 1023$ K; *2* — $n_{HCl} = 3.3$ mol l^{-1}; *3* — $n_{HCl} = 4.9$ mol l^{-1}; *4* — $n_{HCl} = 8.2$ mol l^{-1} [166].

Let us now consider the structure of individual crystals, for instance, those of muscovite [183]. In such a crystal, two layers of SiO_4^{4-} anionic groups bound to aluminium ions form layers oriented perpendicular to the axis *C*. A part of the potassium nests in muscovite and phlogopite crystals are occupied by water molecules, whereas some interpacket zones contain monomolecular water interlayers [168].

Given the close layer packing, the electronic shells of oxygen ions belonging to SiO_4^{4-} anions and adjacent H_2O molecules may be assumed to overlap. Such assumption is supported by observations of calcium sulfate crystalline hydrate, a layered crystal [184]. This would ease both proton passage over the barrier and proton tunnelling from an H_3O^+ ion formed in the water layer to the nearest SiO_4^{4-} anion. In this case, a change of orientation is a necessary condition for further movement of the charge carrier. A change in SiO_4^{4-} orientation due to a turn of the whole anion is unlikely. The reorientation of a protonated $HSiO_4^{3-}$ anion is much more probable due to proton transfer from one oxygen ion to another inside the anion, as was demonstrated for sulfate crystalline hydrates in Refs [182, 185, 186, 166].

The reorientation of the $HSiO_4^{3-}$ anion being completed, the proton moves to adjacent SiO_4^{4-} anion. This passage along a hydrogen bond does not involve activation and is realized by the tunnelling mechanism at a rate of 10^{13} s^{-1}, which is considerably higher than $1/\tau$, where τ is the relaxation time [166]. Therefore, a proton repeatedly passes from one anion to another in a time of the favourable-for-proton-transfer orientation, which means that the proton charge is equally distributed between them. Also, it seems quite likely that OH^- ions participate in proton transfer between the layers.

Migration of H_3O^+ defects between electrodes and across the sample is actually a sequence of events including

— formation of H_3O^+ defects;

— proton movement from the H_3O^+ ion to SiO_4^{4-} anion and the formation of a protonated $HSiO_4^{3-}$ anion;

— reorientation of the protonated anion due to a proton transfer inside it;

— proton movement between cells of the anionic sublattice, with a newly formed protonated anion acquiring the opposite orientation;

— reorientation of the second protonated anion, and

— proton migration to a water molecule and the formation of an H_3O^+ defect:

$$HSiO_4^{3-} + H_2O \rightarrow SiO_4^{4-} + H_3O^+ .$$

Migration of OH^- ions proceeds in the same manner with the sole exception that it has the opposite direction (Table 4).

The contribution of L- and D-defects and VL and VD complexes to electric conductivity is insignificant. The mechanism of their movement between layers is likely to be different only at an early stage, when orientation defects are being formed, because a proton can pass to a SiO_4^{4-} anion only after a turn of the water molecule.

To summarize, the migration of defects in layered sulfate and silicate crystalline hydrates is due to proton movement through the crystal giving rise to protonated anions. Therefore, rotations of H_3O^+ and OH^- ions and H_2O dipoles are supported by the migration of protons which are responsible for dielectric relaxation. Dipole migration to a neighbouring vacancy with a turn in the direction of the field, i.e. relaxation of polar vacancies described in Ref. [2], is possible in principle but hardly occurs in reality, as the calculations in [2] demonstrate.

5.4 Low-temperature relaxation

The relaxation process at low temperatures develops in protonated $HSiO_4^{3-}$ anions. Their relaxation results in proton migration from one oxygen ion to another both inside and between the anions. For this reason, the current generated by the relaxation of $HSiO_4^{3-}$ anions is rather small. The activation energy must be equally low because proton movement is possible not only by activation but also due to the tunnelling effect [166]. The travelling molecules come close to one another, and the probability of proton tunnelling increases [187].

Statistical analysis of experimental findings has revealed a weak maximum ($I = 10^{-13} - 10^{-14}$ A) with an activation energy of 0.05 eV (see Table 3) in the TSDC spectrum of phlogopite at around 100 K (see Fig. 21). A similar peak for talc has an activation energy of 0.06 eV at $T = 86$ K. The peak enhances with increasing the concentration of HCl impurity.

This TSDC maximum was not displaced after annealing crystals, whereas other peaks disappeared. Only at the annealing temperature over 1200 K (for phlogopite), when both all water and part of the protons were evolved [168], peak 1 came almost to nought. It was therefore concluded that the peak was due to the relaxation of an anionic sublattice, specifically that of protonated anions $HSiO_4^{3-}$ (in silicates) and HSO_4^- (in sulfate crystalline hydrates). The estimated concentration of protonated $HSiO_4^{3-}$ anions was of order 10^{16} m^{-3} (Table 5).

Table 5. Defect concentration in phlogopite.

Peak No.	T_m, K	Concentration n, m^{-3}
1	100	1.2×10^{16}
2	130	4.3×10^{16}
3	178	2.0×10^{18}
4	206	3.0×10^{17}
5	235	2.2×10^{18}
6	260	5.0×10^{18}
7	405	3.5×10^{20}

It is possible to examine the potential by the quasi-classical method provided the condition $m\omega\delta^2/4\hbar \gg 1$ is satisfied. This requirement is met in the case being considered. To judge the transmission coefficient, let us approximate the potential relief using a one-dimensional rectangular barrier for which the conditions $2mU(x)/\hbar^2 = K_0^2$ at $|x| \leqslant a$ and $U = 0$ beyond this interval are fulfilled. Then we arrive at

$$D = \left(1 + \frac{K_0^2}{2K\varkappa}\sinh 2\varkappa a\right)^{-1}, \tag{5.1}$$

where

$$K^2 = \frac{2m}{\hbar^2}E, \quad \varkappa^2 = K_0^2 - K^2, \quad a = \frac{\delta}{2}.$$

Here, E is the proton energy.

The width of the potential barrier can be found in Ref. [165]:

$$U = \frac{m\omega^2\delta^2}{8}, \quad \omega = 2\pi\nu, \quad \nu = 10^{13}\,\mathrm{s}^{-1}. \tag{5.2}$$

Since $U = 0.06$ eV, one obtains $\delta = 1.08 \pm 0.05$ A. The separations between oxygen ions in the SO_4^{2-} anion and between an oxygen ion and a water molecule are 1.215 and 1.35 A, respectively. The interanion distance is 1.4 A. Therefore, the estimated width of the barrier is acceptable.

The energy of proton thermal motion at 92 K does not exceed 0.01 eV, which is insufficient to overcome the potential barrier. Results of calculations using formula (5.2) indicate that the transmission coefficient has a definite value, that is $D = 8.4\times10^{-5}$ at the pedestal of the barrier, taking into account the thermal motion energy, and $D = 7.2\times10^{-3}$ at the mid-height of the barrier, where $E = U/2$. Hence, as many as 8.4×10^{-3}% of the total number of particles incident on the barrier pass at its pedestal compared with 0.72% at the mid-height. In other words, proton migration inside and between SO_4^{2-} anions occurs through tunnelling. This inference is confirmed by experiments using ammonium sulfate and potassium dehydrophosphate crystals [181, 185].

To conclude, peak 1 of the TSDC spectrum is related to relaxation of HSO_4^- (sulfates) or $HSiO_4^{3-}$ (silicates) ions, while the migration of defects in hydrosulfates and hydrosilicates is due to proton movements by relays over the anionic sublattice and water layers.

5.5 Dielectric losses

Figures 26–29 display the $\tan\delta$ and ε' frequency and temperature spectra for talc and gypsum in the temperature range 77 to 350 K. The frequency dependence shows three $\tan\delta$ maxima with the middle one reducing after annealing.

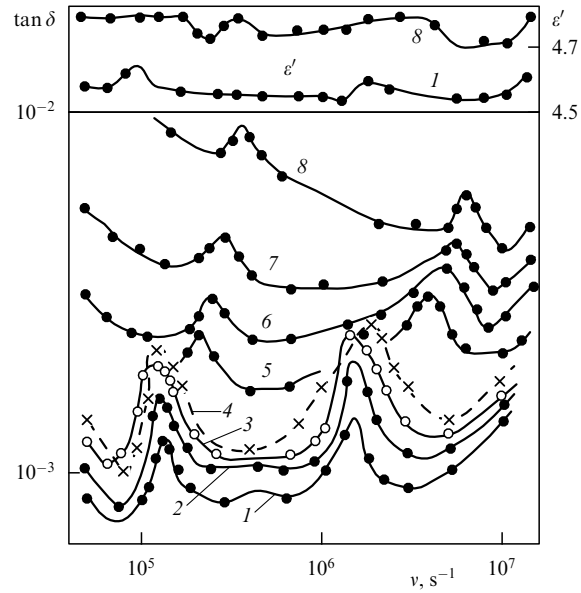

Figure 26. $\tan\delta$ and ε' frequency spectra of talc for $T_{an} = 1023$ K at different temperatures: *1* — 80 K; *2* — 98 K; *3* — 112 K; *4* — 125 K; *5* — 150 K; *6* — 218 K; *7* — 250 K, and *8* — 298 K [166].

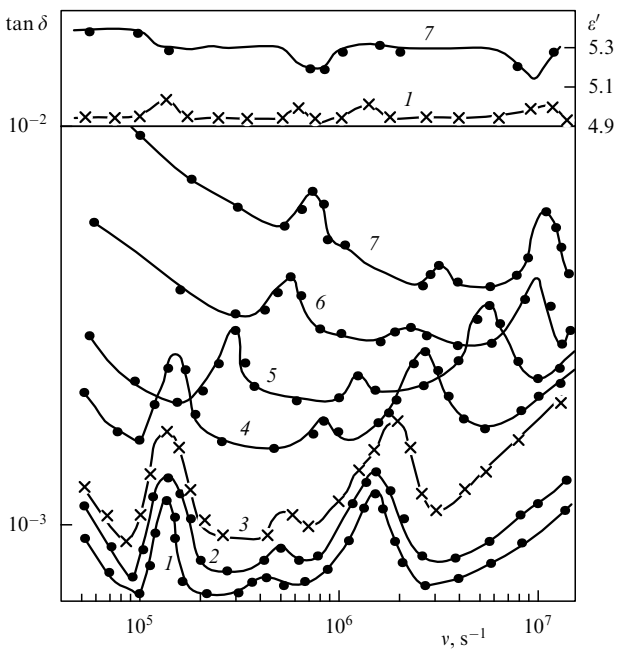

Figure 27. $\tan\delta$ and ε' frequency spectra of gypsum ($CaSO_4\cdot0.5H_2O$) for $T_{an} = 393$ K at different temperatures: *1* — 86 K; *2* — 112 K; *3* — 124 K; *4* — 150 K; *5* — 200 K; *6* — 273 K, and *7* — 293 K [166].

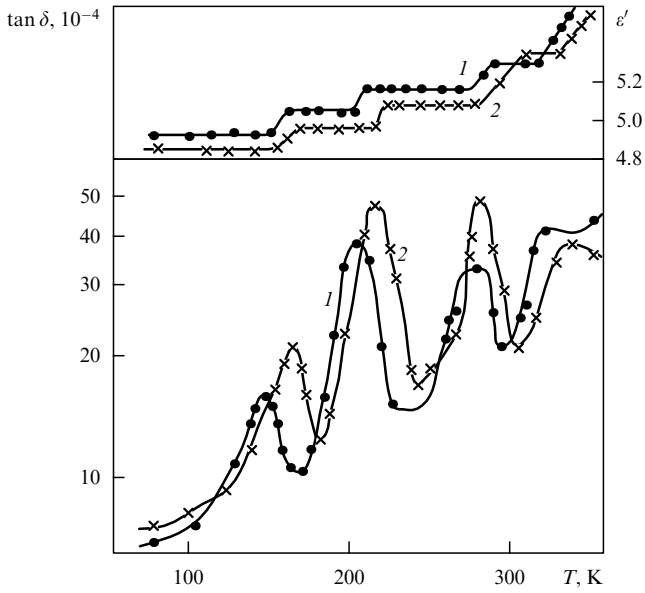

Figure 28. $\tan\delta$ and ε' temperature spectra of gypsum ($CaSO_4 \cdot 0.5H_2O$) for $T_{an} = 393$ K: *1* — $\nu = 7$ MHz, and *2* — $\nu = 12$ MHz [166].

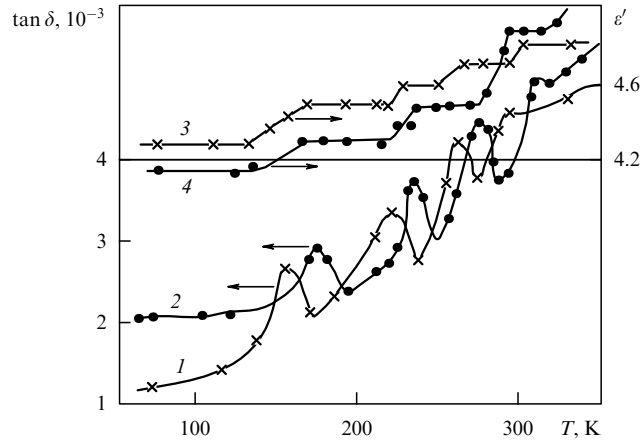

Figure 29. $\tan\delta$ and ε' temperature spectra of talc for $T_{an} = 1023$ K: *1*, *3* — $\nu = 7$ MHz, and *2*, *4* — $\nu = 12$ MHz [166].

A shift of the maxima to the lower frequency region upon a fall in temperature suggests its relaxation nature. The $\varepsilon'(\omega)$ spectrum does not exhibit apparent dispersion regions, which makes it impossible to construct Cole and Cole plots $\varepsilon'' = f(\varepsilon')$, a feature characteristic of ionic crystals [2].

The $\tan\delta$ temperature spectrum has four maxima (see Figs 28, 29).

A shift to the lower temperature region with decreasing frequency from 7 MHz to 1 kHz results in the displacement of peak 1 to below 80 K. The activation energy is calculated from the formula

$$U = \frac{kT_1T_2}{T_2 - T_1} \ln\frac{\omega_2}{\omega_1} . \qquad (5.3)$$

The values of the latter quantity are presented in Table 6. A smaller number of maxima on the $\tan\delta$ temperature curve compared with that for TSDC dependence is due to the release of adsorbed water from samples before the measurement, while the volume charge relaxation fails to appear because of the significant loss for electric conductivity.

Table 6. Activation energies derived from a $\tan\delta = f(T)$ spectrum.

Peak No.	Talc		Gypsum	
	T_m, K	U, eV	T_m, K	U, eV
1	160	0.9±0.02	145	1.10±0.02
2	220	0.18±0.03	210	0.20±0.05
3	265	0.36±0.04	270	0.45±0.07
4	310	0.40±0.08	320	0.6±0.2

In samples previously maintained in a HCl solution, $\tan\delta$ turned out to increase while the maxima shifted to the higher frequency region, but they shifted to the lower frequency region after annealing. The low resolving capacity of the method, in particular, in the low-temperature region where the error sharply raised, did not allow the $\tan\delta$ maximum due to protonated anion relaxation to be identified.

Measurements at a lower-than-critical temperature are affected by the tunnelling effect (see formula 4.23). It follows from the experimental curve $\ln\tau = f(1/T)$ (Fig. 30) that the slope relative to the horizontal axis, which unambiguously defines the activation energy of a given type of relaxator, sharply decreases at the critical point. The height of potential barrier cannot change jumpwise, but its transmission D is altered. And precise calculations are difficult here for mathematical reasons.

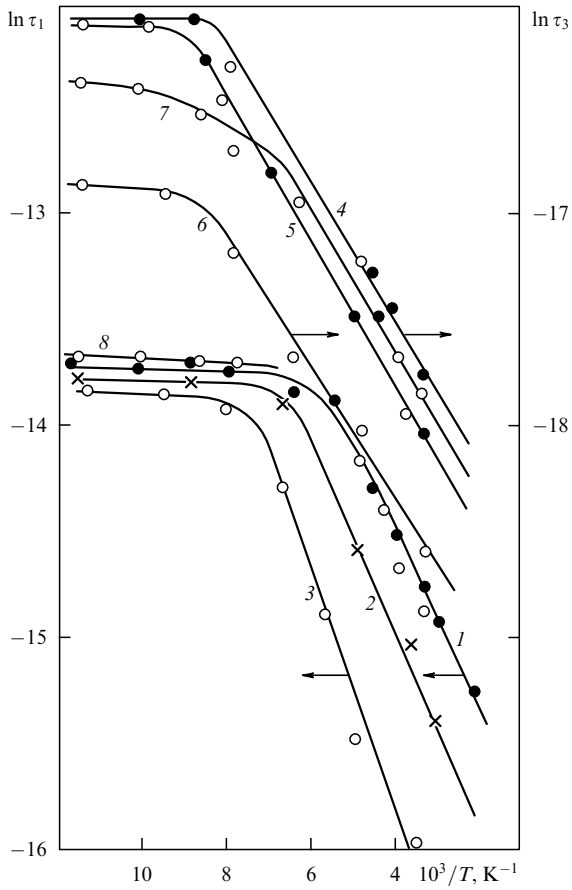

Figure 30. Temperature dependence of relaxation time for dipoles (peaks 1 and 3 in $\tan\delta(T)$ curve): *1*, *4* — talc, $T_{an} = 1023$ K; *2*, *5* — gypsum, $T_{an} = 393$ K; *3*, *6* — natural gypsum, and *7*, *8* — natural talc [166].

A comparison of relaxation times, activation energies, positions of peaks in $\tan\delta(T)$ curve and TSDC density spectrum indicates that the first low-temperature $\tan\delta(T)$ maximum is due to the relaxation of H_3O^+ ions, the second to that of crystallization water dipoles, the third to the relaxation of OH^- ions, and the fourth to the migration of VL and VD complexes [165].

5.6 Theoretical and experimental spectra of thermally stimulated depolarization currents

The above proton relaxation mechanism is consistent with the theory discussed in Section 4.2. Let us compare experimental TSDC spectra of phlogopite with those calculated using formula (4.53).

The physical sense of the summation over k is in the consideration of a set of dipoles differing in the degree of fixation. At $k = 1, 2, 3, \ldots$, Eqn (4.53) gives three closely located maxima each having a smaller amplitude than the previous one. Collectively, these maxima yield one broadened peak for a given type of relaxators. The current density at $k = 3$ is very small already. Hence, the difference between dipole fixation conditions is insignificant for a given sort of dipoles.

Using Eqn (4.53) for each group of relaxators allows the theoretical TSDC density spectrum to be constructed. It is not difficult to find the number of layers $m = d/a = 2.5 \times 10^5$ when the thickness and magnitude of parameter a are known (in other words, m is the effective number of potential wells in the mathematical model). The TSDC density for water molecules is calculated using the effective molecular charge $q_{\text{eff}} = \mu/r_{\text{eff}}$, where μ is the dipole moment, and r_{eff} is the effective radius of the molecule. The computed m value turned out to be of order $(1-5)\times 10^5$.

The theoretical and experimental spectra are nearly identical (Fig. 31). A marked enhancement and shift of experimental peak 7 compared with the theoretical peak are due to the imposed electretic current as mentioned above. There was no such shift in the talc TSDC spectrum [164]. Taking into consideration the electretic current above 220 K, the TSDC density calculated using (4.53) increases and the resultant spectrum correlates fairly well with the experimental one.

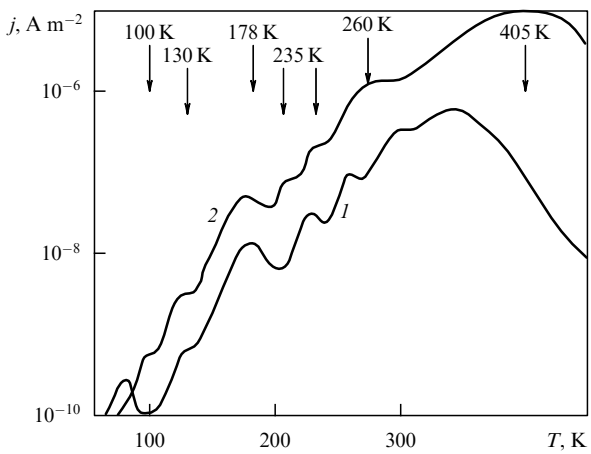

Figure 31. TSDC density spectrum of phlogopite: *1* — calculated by (4.53); *2* — experimental, at $E_p = 10^6$ V m^{-1}, $T_p = 300$ K, $d = 5$ μm, and $c = 0.1$ K s^{-1} [179].

It should be borne in mind that the interpretation of TSC measurements proceeding from the ideal isothermal Debye response in terms of the Bucci and Fieschi theory [1] refers to a rough approximation as was emphasized by Jonscher [188]. The proposed theory is devoid of this drawback since it leans upon a solution of the system of kinetic equations (4.35) and therefore reflects the relaxation process in full (in the framework of the Boltzmann approximation for determining the relaxator concentration). The relaxation mechanism remains virtually the same as in ice, that is the relaxing defects of H_3O^+, OH^-, L, D, VL and VD complexes, and protonated anions are oriented in the electric field by virtue of proton migration along hydrogen bonds.

To sum up, the proposed method for dielectric spectroscopy including complex measurements of TSDC, TDC, $\tan\delta$, ε', γ, τ and computation of TSC density based on the kinetic relaxation theory [Eqn (4.53)] gives an adequate approximation to the description of dielectric relaxation.

6. Conclusions

The present review summarizes results of proton relaxation and carrier transport studies in ice and inorganic crystals containing water and OH^- radicals, by dielectric spectroscopy from a single standpoint. Until recently, studies along these lines have been developing independently, thus leading to mistakes and misunderstanding. For instance, calculations of $\tan\delta$ in crystalline hydrates disregarded the relaxation of Bjerrum defects and thus failed to provide results in conformity with experiment [2]. The universally accepted explanation for the temperature and frequency dependences of $\tan\delta$ was inadequate since it took account of H_2O, OH^- dipoles but ignored L- and D-defects and H_3O^+ ions [2].

The construction of a rigorous theory of dielectric loss and TSCs in hydrogen-bonded crystals encounters serious difficulties pertinent to computation. Specifically, calculating the relaxation of orientation defects in the crystal lattice of hexagonal ice at the molecular level yields results which are difficult to interpret even if the volume charge is disregarded [189].

So far, partial fluxes of ice structural defects (the configuration vector) and quantum effects at low temperatures have not been fully taken into consideration. One has to reconcile oneself with the multiwell potential relief model described in this review, which very nearly approximates the real structure in the case of crystalline hydrates and micas. These calculations qualitatively correspond to the experimental findings and define the boundary between Debye and quantum relaxations.

The most important conclusion from the analysis of the scientific literature in the present review is that hydrogen-bonded crystals are proton semiconductors and dielectrics having a common mechanism of proton relaxation by means of their migration along hydrogen bonds with different activation energies and charges $0.38e$ and $0.62e$. Other relaxation processes largely occur in the quantum region (the relaxation of $HSiO_4^{-3}$ and HSO_4^- ions). Volume charge relaxation remains to be investigated, and the origin of the charge is virtually unknown. It appears safe to state that the electretic state arises in hydrogen-bonded crystals through the relaxation of Bjerrum defects, especially that of OH^- ions. This concept questions the possibility of ferroelectrical phenomena in ice.

A strict theory of proton relaxation in hydrogen-bonded crystals is needed to better understand nonlinear polarization effects, primarily the mechanism of electretic state formation and quantum polarization [190].

The technological utility of these effects is quite obvious.

Acknowledgments. I wish to thank my co-workers for their help in research on the problem covered by this review. Special thanks are due to È A Aziev, K Zh Birzhanov, V A Mironov, V Ya Medvedev, and V M Timokhin.

References

1. Bucci G, Fieschi R *Phys. Rev. Lett.* **12** (1) 91 (1964)
2. Tonkonogov M P, Mironov V A *Izv. Vyssh. Uchebn. Zaved., Fiz.* (1) 122 (1979)
3. Tonkonogov M P *Dièlektricheskaya Relaksatsiya, Elektricheskiĭ Proboĭ i Razrushenie Gornykh Porod* (Rock Dielectric Relaxation, Electric Breakdown, and Destroy) (Moscow: Nedra, 1975)
4. Leshchenko M A, Poplavko Yu M *Ukr. Fiz. Zh.* **37** (6) 898 (1992)
5. Valenkevich V A, Metsik M S, Gudkov O I *Izv. Vyssh. Uchebn. Zaved., Fiz.* (3) 37 (1982)
6. Gränicher H *Z. Kristallogr.* **110** 432 (1958)
7. Gränicher H, Jona F *Helv. Phys. Acta Suppl.* **5** 50 (1960)
8. Peterson S W, Levy H A *Acta Crystallogr.* (10) 70 (1957)
9. Steinemann A *Helv. Phys. Acta* **30** 581 (1957)
10. Gorokhovatskiĭ Yu A *Osnovy Termodepolyarizovannogo Analiza* (Fundamentals of Thermodepolarization Analysis) (Moscow: Nauka, 1981)
11. Auty R P, Cole R H *J. Chem. Phys.* **20** (8) 1309 (1952)
12. Humbel F, Jona F, Scherrer P *Helv. Phys. Acta* **26** 17 (1953)
13. Glockman H P, in *Proc. Symp. on Physics of Ice* [Münich (W. Germany), 1969] p. 502
14. Johari G P, Whalley E *J. Chem. Phys.* **75** (3) 1333 (1982)
15. Kawada S *J. Phys. Soc. Jpn.* **44** (6) 1881 (1978)
16. Kawada S *J. Phys. Soc. Jpn.* **47** (6) 1850 (1979)
17. Mounier S, Sixou P, in *Proc. Symp. on Physics of Ice* [Münich (W. Germany), 1969] p. 562
18. Ruepp R, Käb M D, in *Physics of Ice* (New York: Plenum, 1969) p. 555
19. Worz O, Cole R H *J. Chem. Phys.* **20** 1309 (1952)
20. Bradley R S *Trans. Faraday Soc.* **53** 687 (1957)
21. Camp P R, Kizenick W, Arnold D, in *Physics of Ice* (New York: Plenum, 1969) p. 450
22. Eigen M L, de Maeyer L, Spatz H C, in *Colloquium on the Physics of Ice Crystals* (Zurich: Erlenback, 1962)
23. Camplin G C, Glen G W, Paren J G *J. Glaciology* **21** (85) 123 (1978)
24. Von Hippel A et al. *J. Chem. Phys.* **57** (6) 2561 (1972)
25. Jaccard C *Helv. Phys. Acta* **32** 89 (1959)
26. Johnstone J H L *Trans. Nova Scotia Inst.* **13** 126 (1912)
27. Takei L, Maeno N, in *Abstracts VIIth Symposium on Physics and Chemistry of Ice* [Grenoble (France), September 1986] p. 73
28. Bernal J D, Fowler R H *J. Chem. Phys.* **1** 515 (1933)
29. Gianque W F, Stout J W *J. Am. Chem. Soc.* **58** 1144 (1936)
30. Meijering J L *Phillips Res. Rep.* (12) 333 (1957)
31. Pauling L *J. Am. Chem. Soc.* **57** 2680 (1935)
32. Whalley E, Davidson D W, Heath J B R *J. Chem. Phys.* **45** 3976 (1966)
33. Long E A, Kekp J D *J. Am. Chem. Soc.* **58** 1829 (1936)
34. Bjerrum N K *Dan. Vidensk. Selsk. Mat.-Fys. Medd.* **21** 1 (1951)
35. Chen M S et al. *J. Chem. Phys.* **60** (2) 405 (1972)
36. Kuhn W, Thürkauf M *Helv. Chem. Acta* **41** 938 (1958)
37. Thürkauf M *Thesis,* University of Basel (1956)
38. Gränicher H, in *Physics of Ice* (New York: Plenum, 1969) p. 1
39. Gränicher H *Z. Kristallogr.* **110** 450 (1958)
40. Jaccard C *Phys. Kondens. Mater.* **3** 99 (1964)
41. Bilgram J H, Gränicher H *Phys. Kondens. Mater.* **18** 275 (1974)
42. Steinemann A, Gränicher H *Helv. Phys. Acta* **30** 553 (1957)
43. Camplin G C, Glen J W, in *Papers presented at the Symposium on the Physics and Chemistry of Ice* (Ottawa, 1973) p. 256
44. Gränicher H, in *Physics of Ice* (New York: Plenum, 1969) p. 492
45. Nagle J F *J. Glaciology* **21** 315 (1978)
46. Ruepp R, in *Papers presented at the Symposium on the Physics and Chemistry of Ice* (Ottawa, 1973) p. 179
47. Taubenberger R, Hubmann M, Gränicher, in H *Papers presented at the Symposium on the Physics and Chemistry of Ice* (Ottawa, 1973) p. 194
48. Eigen M, de Mauer L *Z. Electrochem.* **60** 1037 (1956)
49. Boned C, Barbier A, in *Papers presented at the Symposium on the Physics and Chemistry of Ice* (Ottawa, 1973) p. 208
50. Camp P R, Kiszenik W, Arnold D, in *Proc. Symposium on Physics of Ice* [Münich (W. Germany), 1969] p. 52
51. Itagaki K, in *Abstracts VIIth Symposium on Physics and Chemistry of Ice* [Grenoble (France), September 1986] p. 92
52. Klinger J, in *Papers presented at the Symposium on the Physics and Chemistry of Ice* (Ottawa, 1973) p. 114
53. Worz O, Cole R H *J. Chem. Phys.* **51** (4) 1546 (1969)
54. Gough S R, Davidson D W *J. Chem. Phys.* **52** 5442 (1970)
55. Owston P G *Adv. Phys.* **7** 171 (1958)
56. Barnaal D E, Love I J *J. Chem. Phys.* **48** 4614 (1968)
57. Krüger G J *Thesis* (Stuttgart: Technische Hochschule, 1961)
58. Simon F E, in *Handbuch der Physik* **10** 363 (1926)
59. Wollan E A, Davidson D W, Shul C G *Phys. Rev.* **94** 1073 (1954)
60. Johari G P, Jones S J *J. Chem. Phys.* **62** (10) 4213 (1975)
61. Johari G P, Jones S J *Proc. Roy. Soc. A* **349** 467 (1976)
62. Johari G P, Jones S J *J. Glaciology* **21** 259 (1978)
63. Kawada S, Ninuma J *J. Phys. Soc. Jpn.* **43** 715 (1977)
64. Onsager L, Dupuis M, in *Proc. Int. Symp. on Electrolytes* (Trieste – Oxford, June 1959) p. 27
65. Haida O, Suga H, Seki S, in *Proc. Jpn. Acad. Sci.* **49** 191 (1975)
66. Haida O et al. *J. Chem. Thermodyn. G* **815** (1974)
67. Haida O, Suga H, Seki S *J. Glaciology* **22** 155 (1978)
68. Van den Beukel A *Phys. Status Solidi* **28** 565 (1968)
69. Matsuo T et al., in *Papers presented at the Symposium on the Physics and Chemistry of Ice* (Ottawa, 1973) p. 272
70. Pick M A, Wenzl H, Engelhardt H *Z. Naturforsch. A* **26** 810 (1971)
71. Hubmann M *Z. Phys. B* **32** 127 (1973)
72. Kryachko B S *Fiz. Tverd. Tela* **29** (2) 345 (1987) [*Sov. Phys. Solid State*]
73. Cohan N V et al. *Trans. Faraday Soc.* **58** 490 (1962)
74. Dunitz J D *Nature* (London) **197** 862 (1963)
75. Eisenberg D, Coulson C A *Nature* (London) **199** 368 (1963)
76. Hubmann M *Z. Physik B* **32** 141 (1979)
77. Taubenberger R, in *Papers presented at the Symposium on the Physics and Chemistry of Ice* (Ottawa, 1973) p. 187
78. Dantl G, Gregora I *Naturwiss. Enschaften* **55** 176 (1968)
79. Dantl G *Phys. Kondens. Mater.* (7) 390 (1968)
80. Siegle G, Weithaze M *Z. Phys.* **219** 364 (1969)
81. Barbier A *Thèse Doctorat ès Sciences Physiques* (Universite de Pau, 1971)
82. Barbier A *Thèse Doctorat ès Sciences Physiques* (Universite de Pau, 1972)
83. Cazaban-Marque R *Thèse Doctorat ès Sciences Physiques* (Universite de Pau, 1972)
84. Evrard G *Thèse Doctorat ès Sciences Physiques* (Universite de Pau, 1971)
85. Lafarque C, Babin L, in *Proc. XIIth Colloque Ampere* Vol. 9 (Bordeaux, 1963) p. 374
86. Le Petit J P *Thèse Doctorat ès Sciences Physiques* (Universite de Pau, 1971)
87. Jellinek H H G *J. Colloid Interface Sci.* **25** 192 (1967)
88. Nakaya V, Matsumoto A *U.S. Army Snow Ice and Permafrost Res. Estab. Res. Paper* 4 (1953)
89. Weyl W A *J. Colloid Sci.* (6) 389 (1951)
90. Clausse M *Acad. Sci. Paris B* **274** 649 (1972)
91. Khanai T *Kolloidn. Zh.* **171** 23 (1960)
92. Bell J P, Myat R W, Richards R E *Nature* (London) **230** 91 (1971)
93. Dupuy D *Thèse Doctorat ès Sciences Physiques* (Universite de Grenoble, 1970)
94. Tiller W A *J. Cryst. Growth* (6) 77 (1969)
95. Young G, Salomon R E *J. Chem. Phys.* **48** (4) 1635 (1968)
96. Zaretskii A V, in *Abstracts VIIth Symposium on Physics and Chemistry of Ice* [Grenoble (France), September 1986] p. 48
97. Apecis L, Pissis P, in *Abstracts VIIth Symposium on Physics and Chemistry of Ice* [Grenoble (France), September 1986] p. 56

98. Cole R H, Worz O, in *Proc. Symp. on Physics of Ice* [Münich (W. Germany), 1969] p. 546
99. Von Hippel A *J. Chem. Phys.* **54** (1) 145 (1971)
100. Takel I, Maeno M *J. Chem. Phys.* **81** (12) 6186 (1984)
101. Zaretskii A V et al., in *Abstracts VIIth Symposium on Physics and Chemistry of Ice* [Grenoble (France), September 1986] p. 49
102. Breckenridge R G *J. Chem. Phys.* **18** 913 (1950)
103. Breckenridge R G, in *Imperfections in Nearly Perfect Crystals* (New York: Wiley, 1952) p. 219
104. Gross G W *Ann. N.Y. Acad. Sci.* **165** 380 (1965)
105. Levi L, in *Proc. Symp. Physics of Snow and Ice* [Sapporo (Japan), 1967] p. 159
106. Bilgram J H, Wenzl H, Mair G *J. Cryst. Growth* **20** 319 (1973)
107. Engelhardt H, in *Papers presented at the Symposium on the Physics and Chemistry of Ice* (Ottawa, 1973) p. 226
108. Gränicher H, in *Physics of Ice* (New York: Plenum, 1969) p. 1
109. Ryzhkin I, in *Abstracts VIIth Symposium on Physics and Chemistry of Ice* [Grenoble (France), September 1986] p. 51
110. Onsager L, in *Physics of Ice* (New York: Plenum, 1969) p. 363
111. Von Hippel A, Knoll D B, Westphal W B *J. Chem. Phys.* **54** (1) 134 (1971)
112. Zaromb S, Brill R *J. Chem. Phys.* **24** 895 (1956)
113. Petrenko V F, Ryzhkin I A *Zh. Eksp. Teor. Fiz.* **93** (8) 558 (1987) [*Sov. Phys. JETP* **66** 400 (1987)]
114. Aziev È A et al., Preprint No. T-25011 (Chernogolovka: IFTT AN SSSR, 1987)
115. Chai S Y, Vogelhut P O *Science* **148** 1595 (1965)
116. Sutherland B, Yang C N, Yang C P *Phys. Rev. Lett.* **19** 588 (1967)
117. Gross G W *Science* **138** 520 (1962)
118. Gränicher H et al. *Discuss. Faraday Soc.* **23** 50 (1957)
119. Gränicher H *Phys. Kondens. Mater.* **1** 1 (1963)
120. Hammer C H, in *Abstracts VIIth Symposium on Physics and Chemistry of Ice* [Grenoble (France), September 1986] p. 73
121. Heinmets F, Blum R *Trans. Faraday Soc.* **59** 1141 (1963)
122. Petrenko V F, Ryzhkin I A *Phys. Status Solidi B* **121** 421 (1984)
123. Itagaki K, in *Abstracts VIIth Symposium on Physics and Chemistry of Ice* [Grenoble (France), September 1986] p. 91
124. Petrenko V F, Khusnatdinov N N, Zaretskii A V, in *Abstracts VIIth Symposium on Physics and Chemistry of Ice* [Grenoble (France), September 1986] p. 41
125. Engelhardt H *Ph.D. Thesis* (Münich: Technische Hochschule, Physics Department, 1965)
126. Krishnan P N, Young I, Salomon R E *J. Phys. Chem.* **70** 1595 (1966)
127. Decroly J C, Gränicher H, Jaccard C *Nature* (London) **30** 465 (1963)
128. Workmann E J, Truby F J, Drost-Hunsen W *Phys. Rev.* **94** 1073 (1954)
129. Oplatka G *Helv. Phys. Acta* **6** 198 (1933)
130. Jobbe G *Ann. Phys.* **16** 217 (1933)
131. MacDonald J R *J. Chem. Phys.* **23** 2308 (1955)
132. Flether N H, in *Papers presented at the Symposium on the Physics and Chemistry of Ice* (Ottawa, 1973) p. 132
133. Maeno N, in *Papers presented at the Symposium on the Physics and Chemistry of Ice* (Ottawa, 1973) p. 140
134. Tonkonogov M P et al. *Izv. Vyssh. Uchebn. Zaved., Fiz.* (10) 72 (1986)
135. Apecis L, Pissis P, Bondouris G *Nuovo Cimento* **20** (3) 932 (1983)
136. Apecis L, Pissis P, Bondouris G *J. Phys. Chem.* **87** (21) 4019 (1983)
137. Apecis L, Pissis P, Bondouris G *Nuovo Cimento* **26** (2) 365 (1981)
138. Pissis P, Bondouris G *Z. Naturforsch.* **360** (10) 321 (1981)
139. Pissis P et al. *Z. Naturforsch. Teil A* **37** (8) 1000 (1982)
140. Pissis P et al. *J. Phys. Chem.* **87** (21) 4034 (1983)
141. Pissis P, Apecis L, Christodoulides C, in *Abstracts VIIth Symposium on Physics and Chemistry of Ice* [Grenoble (France), September 1986] p. 73
142. Dengel O et al. *Phys. Lett.* **9** (4) 291 (1964)
143. Pick M A, in *Physics of Ice* (New York: Plenum, 1969) p. 344
144. Helmreich D, in *Physics of Ice* (New York: Plenum, 1969) p. 231
145. Bishop P G, Glen G W *Nuovo Cimento D* **2** (3) 492 (1983)
146. Engelhardt H, Bullemer B, Riehl N, in *Physics of Ice* (New York: Plenum, 1969) p. 430
147. Engelhardt H, Riehl N *Phys. Kondens. Mater.* **5** 73 (1966)
148. Mascarenhas S, in *Physics of Ice* (New York: Plenum, 1969) p. 483
149. Engelhardt H, Riehl N *Phys. Lett.* **14** (1) 20 (1965)
150. Chamberlain J S *Phys. Kondens. Mater.* **12** 193 (1971)
151. Jeneveau A, Sixou P, Dansas P *Phys. Kondens. Mater.* **14** 252 (1972)
152. Mascarenhas S, Arguello C *J. Electrochem. Soc.: Solid-St. Sci.* **115** 386 (1968)
153. Aziev È A et al., Preprint No. T-25012 (Chernogolovka: IFTT AN SSSR, 1987)
154. Bucci C, Fieschi R, Guidi G *Phys. Rev.* **148** 817 (1966)
155. Pissis P et al. *Z. Naturforsch. Teil A* **36** 321 (1981)
156. Bishop P G, Glen J W, in *Physics of Ice* (New York: Plenum, 1969) p. 492
157. Zaretskii A V et al. *J. Phys.* (*Paris*) **48** (3) 87 (1987)
158. Tonkonogov M P et al. *Zavod. Lab.* (12) 61 (1989)
159. Tonkonogov M P et al. *Izv. Vyssh. Uchebn. Zaved., Fiz.* (12) 3 (1993)
160. MacDonald J R *Phys. Rev.* **92** (1) 4 (1953)
161. Tonkonogov M P, Veksler V A, Orlova E F *Izv. Vyssh. Uchebn. Zaved., Fiz.* (2) 6 (1984)
162. Tonkonogov M P, Medvedev V Ya *Izv. Vyssh. Uchebn. Zaved., Fiz.* (2) 36 (1987)
163. Medvedev V Ya, Tonkonogov M P *Izv. Vyssh. Uchebn. Zaved., Fiz.* (11) 71 (1990)
164. Mironov V A, Timokhin V M, Tonkonogov M P *Izv. Vyssh. Uchebn. Zaved., Fiz.* (1) 68 (1991)
165. Timokhin V M, Tonkonogov M P *Izv. Vyssh. Uchebn. Zaved., Fiz.* (7) 104 (1991)
166. Timokhin V M, Tonkonogov M P, Mironov V A *Izv. Vyssh. Uchebn. Zaved., Fiz.* (11) 82 (1990)
167. Winchell A., Winchell H *The Microscopical Characters of Artificial Inorganic Solid Substances: Optical Properties of Artificial Minerals* (New York; Plenum, 1964) [Translated into Russian (Moscow: Mir, 1967)]
168. Metsik M S *Termicheskie Svoĭstva Kristallov Slyud* (Thermal Properties of Mica Crystals) (Irkutsk: Irkutsk Univ. Publ., 1989)
169. Metsik M S, Shcherbachenko L A *Èlektricheskie Svoĭstva Slyud* (Electrical Properties of Micae) (Irkutsk: Irkutsk Univ. Publ., 1990)
170. Zapol' B A, Alkenis F F *Zh. Prikl. Spektrosk.* **27** (4) 731 (1977)
171. Tonkonogov M P, Timokhin V M USSR Author's Certificate No. 642354, MKI 5 G 01N27/24; *USSR Byull. Izobret.* (14) (1991)
172. Kröger F *The Chemistry of Imperfect Crystals* (Amsterdam: North-Holland, 1964) [Translated into Russian (Moscow: Mir, 1969)]
173. Haas C *Phys. Lett.* **3** 126 (1962)
174. Gubkin A N, Ogloblin N A *Èlektretnyĭ Effekt i Elektricheskaya Relaksatsiya* (Electretic Effect and Electrical Relaxation) (Moscow: MIEM, 1979) p. 150
175. Gubkin A N *Èlektrety* (Electrets) (Moscow: Nauka, 1978)
176. Gross B *Phys. Rev.* **66** 26 (1944)
177. Sessler G M *Electrets* (Berlin: Springer-Verlag, 1980)
178. Tonkonogov M P et al., in *Tez. Dokl. Mezhdunar. Konf. 'Dièlektriki-93'* Ch. 1 (Abstracts of Int. Conf. 'Dielectrics-93', Part 1) (St.-Petersburg: St.-Petersburg State Tech. Univ. Publ., 1993) p. 96
179. Timokhin V M, Tonkonogov M P, Pashkevich A I *Izv. Vyssh. Uchebn. Zaved., Fiz.* (9) 59 (1993)
180. Gemant A *Rev. Sci. Instrum.* **11** (2) 65 (1940)
181. Betekhtin A G *Kurs Mineralogii* (The Course on Mineralogy) (Moscow: Izdatel'stvo po Geologii i Okhrane Nedr, 1956)
182. Khaĭretdinov È F, Burshteĭn A I, Boldyrev V V *Fiz. Tverd. Tela* **15** (10) 3029 (1973) [*Sov. Phys. Solid State*]
183. Berry L, Mason B, Dietrich R *Mineralogy* (San Francisco: Freeman, 1983) [Translated into Russian (Moscow: Mir, 1987)]
184. Wooster W A *Z. Kristallogr. B* **94** 375 (1936)
185. Burshteĭn A I *Usp. Khim.* **17** (2) 212 (1978)
186. Kreuer Klaus-Dieter *J. Mol. Structure* **177** 256 (1988)
187. Tonkonogov M P, Veksler V A, Orlova E F *Izv. Vyssh. Uchebn. Zaved., Fiz.* (1) 97 (1982)
188. Jonscher A K *J. Phys. D* **24** (9) 1633 (1991)
189. Tonkonogov M P et al. *Izv. Vyssh. Uchebn. Zaved., Fiz.* (2) 93 (1994)
190. Tonkonogov M P, Veksler V A, Orlova E F, in *Proc. 5th Int. Symp. Electricity* (New York, 1985) p. 224